Detailed Kinetic Mechanism for the Oxidation of Ammonia Including the Formation and Reduction of Nitrogen Oxides.

Krishna P. Shrestha[1], Lars Seidel[3], Thomas Zeuch[2] and Fabian Mauss[1]

1 Thermodynamics and Thermal Process Engineering, Brandenburg University of Technology, Siemens-Halske-Ring 8, 03046 Cottbus, Germany

2 Institut für Physikalische Chemie, Georg-August-Universität Göttingen, Tammannstraße 6, D-37077 Göttingen, Germany

3 LOGE Deutschland GmbH, Burger Chaussee 25, 03044 Cottbus, Germany

Krishna P. Shrestha, e-mail: shrestha@b-tu.de

Supporting Information also consist of chemical kinetic mechanism, which can be found at

https://data.mendeley.com/datasets/25zw5d5ttw/2

with regular update.

Cite this work as: *Energy Fuels* 2018, 32, 10, 10202–10217,

https://doi.org/10.1021/acs.energyfuels.8b01056

Supporting Information

1. Numerical model used for simulation

1.1 Laminar premixed Flame

The laminar flame speed and species prediction in burner stabilized premixed flame are performed by using the mixture average transport model. The mixture average transport model assumes the same diffusion coefficients for all the species in the flame. For calculating laminar flame speed freely propagating flame setup is used and for speciation and temperature profile in burner stabilized flame burner stabilized flame setup is used in LOGEsoft [1] which solves

the conservation of momentum equation, conservation of species equation and the conservation of energy equation. More details can be found on LOGEsoft manual.

Gridding

Minimum discretization size [m] = 1.0e-9

Maximum discretization size [m] = 0.05

Maximum number of grid points per unit curvature = 1.0

Maximum number of grid points per unit gradient = 1.5

Grid smoothness = 0.05

Number of grid points = 301

Maximum number of grid preadaptation during steady state = 4

Solver settings

Maximum number of time steps = 2000

Minimum time step size [s] = 1.0e-10

Maximum time step size [s] = 0.1

Maximum number of full iteration steps = 50

Maximum number of damping levels for converging solution = 10

Maximum number of detailed Newton steps = 20

Relative tolerance limit = 1.0e-6

1.2 Shock Tube (ST)

Shock tubes are modelled as constant volume reactor model with the reflected shock pressure and temperature used as the initial conditions. The ignition delay time is predicted determined as per the definition used in the experiment.

Solver settings

Minimum time step size [s] = 1.0E-010

Maximum time step size [s] = 1.0E-003

Final time [s] = 5.0E-002

Initial time [s] = 0.0

Maximum order of bdf method = 5

Absolute tolerance limit = 1.0E-010

Relative tolerance limit = 1.0E-008

Maximum number of full iteration = 10

Maximum number of damping levels for converging solution = 3

Maximum number of detailed Newton steps = 20

1.3 Jet Stirred Reactor (JSR)

The species profile data from JSR are compared with the predicted species profile from the Perfectly Stirred Reactor (PSR) model setup. The PSR model assumes the constant pressure vessel with inlet and outlet ducts. In the simulation we employed the steady state, constant temperature condition for all the simulation performed.

Solver settings

Minimum time step size [s] = 1.0E-010

Maximum time step size [s] = 1.0E-003

Final time [s] = 10 * residence time

Initial time [s] = 0.0

Maximum order of bdf method = 5

Absolute tolerance limit = 1.0E-010

Relative tolerance limit = 1.0E-008

Maximum number of full iteration = 10

Maximum number of damping levels for converging solution = 3

Maximum number of detailed Newton steps = 20

1.4 Flow Reactor

The species profile from the variable pressure flow reactor are compared with the predicted species profile assuming a constant pressure reactor model. The initial conditions are taken

from the experiment. However, the model assumes perfect and instantaneous mixing of the reactants, which may not be the case during the experiments. As suggested by other authors, the time at which reaction starts in the experiments is not well defined, and it is reasonable to shift the predicted species profiles relative to the measured profiles to account for non-idealities in reaction initiation by various causes. This profile is shifted in time so that the predicted point corresponding to 50% of the fuel disappearance matches that reported experimentally.

Solver settings

Minimum time step size [s] = 1.0E-010
Maximum time stepsize [s] = 1.0E-003
Final time [s] = 10 * residence time
Initial time [s] = 0.0
Maximum order of bdf method = 5
Absolute tolerance limit = 1.0E-10
Relative tolerance limit = 1.0E-08
Maximum number of full iteration = 10
Maximum number of damping levels for converging solution = 3
Maximum number of detailed Newton steps = 20

2. Additional validation for NO_x kinetic model

2.1 Laminar Flame Speed

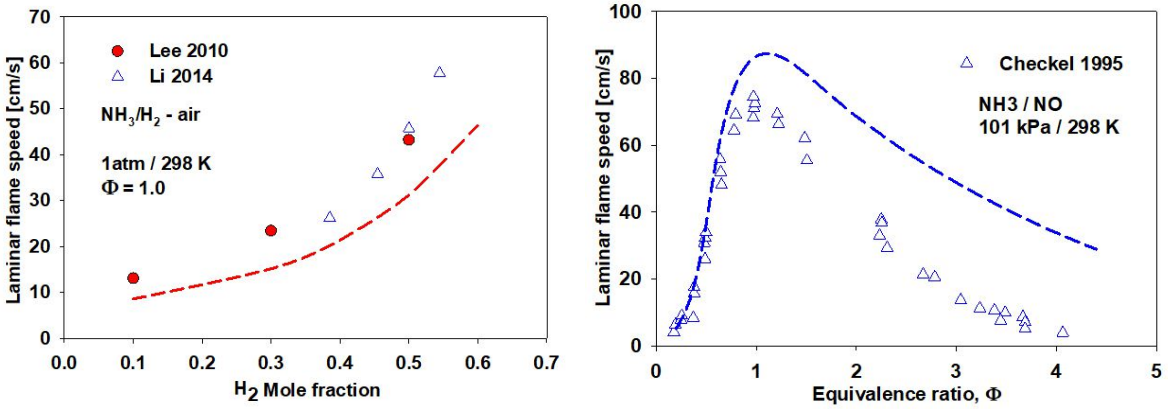

Figure S1: Laminar flame speed Comparison between model predictions against experimental data from literature. Left: NH_3/H_2-air laminar flame speed at ϕ = 1.0, 1atm and 298 K as function of hydrogen fraction, symbols experimental data from [2,3]. Right: NH_3/NO laminar flame speed at 101 kPa and 298 K as function of equivalence ratio, symbols experimental data from [4]. Line: model prediction from this work.

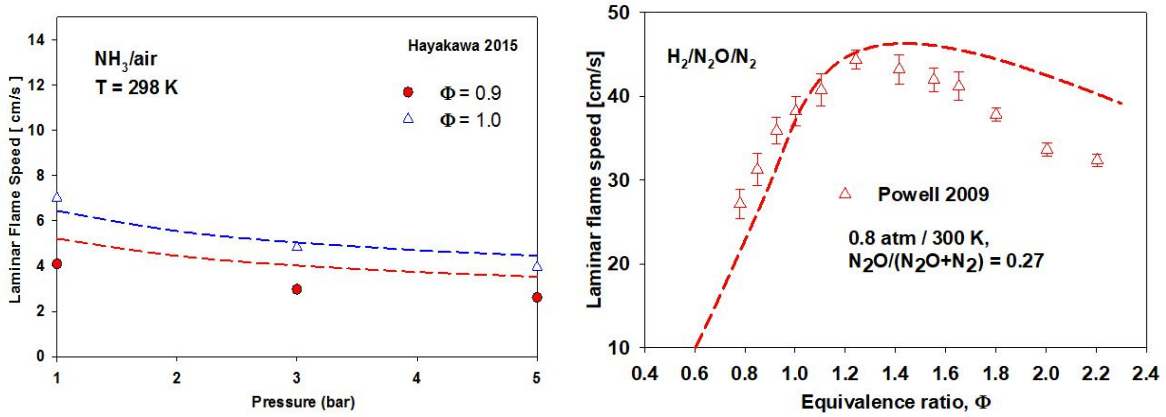

Fig. S2: Laminar flame speed comparison between model prediction against experimental data Left: NH_3/air at 298 K and at different pressure, symbols experiments from [5]; Right: $H_2/N_2O/N_2$ at 0.8 atm and 300 K, symbols experiments from [6], lines model prediction from this work.

2.2 Ignition delay times (Shock Tube)

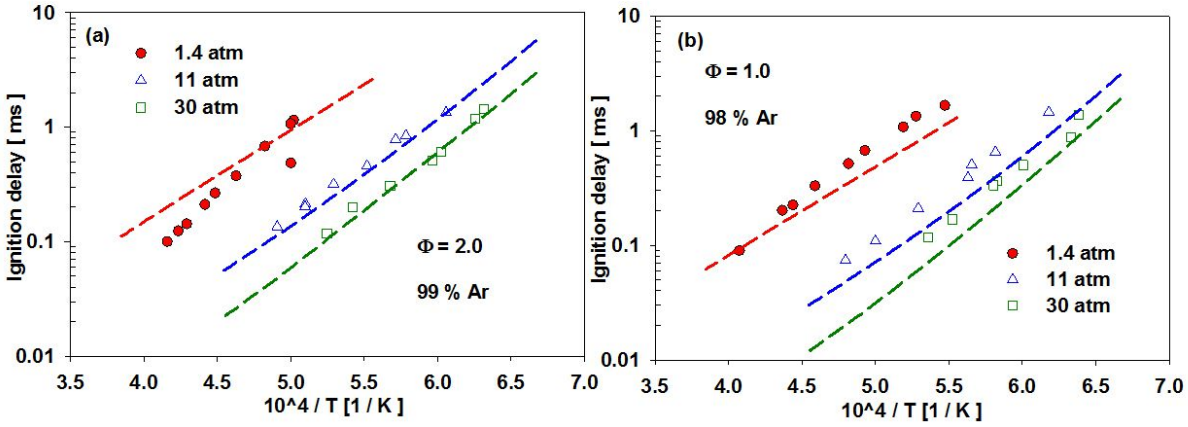

Figure S3: Ignition delay times from shock tube experiments in comparison to model predictions for $NH_3/O_2/Ar$ blends. Symbols: experiments from [7], dashed lines: model predictions.

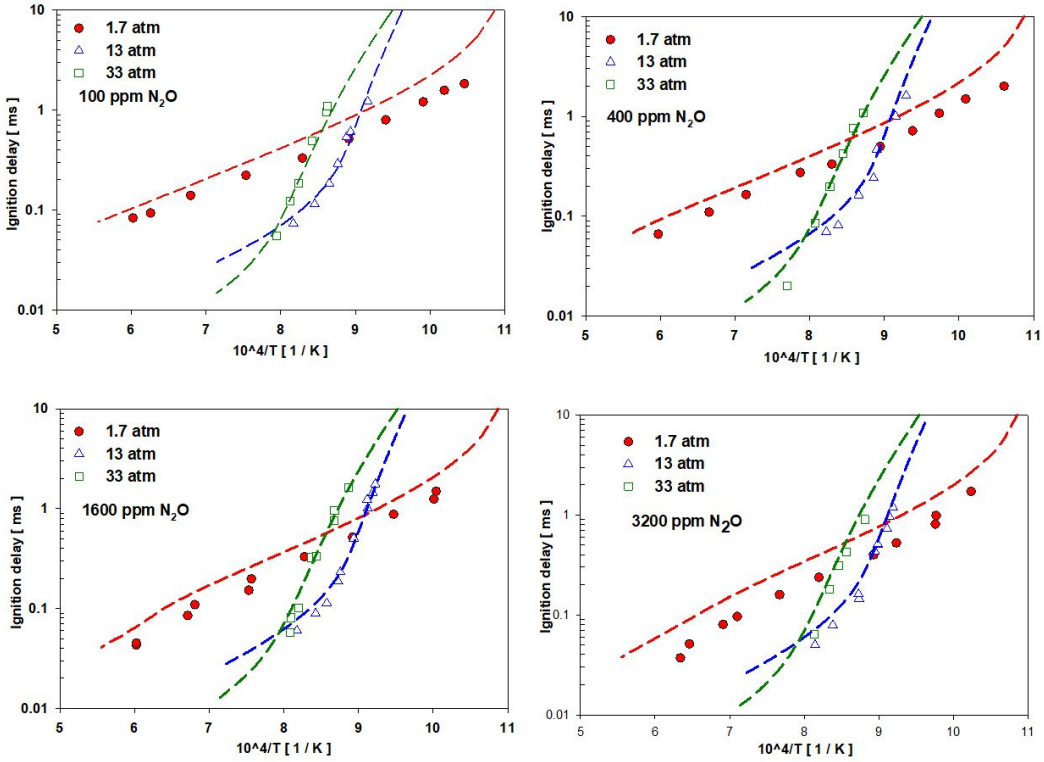

Figure S4: Ignition delay times comparison between model prediction and experimental data for $H_2/O_2/N_2O/Ar$ at varying N_2O (100 ppm – 3200 ppm) concentration. Symbols: experimental data from [8]. Lines: prediction with current model.

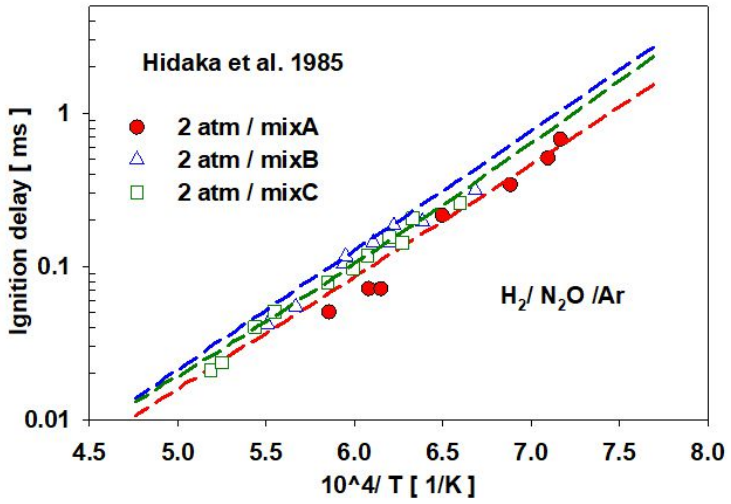

Figure S5: Ignition delay times comparison between model prediction and experimental data for $H_2/N_2O/Ar$ mixture at 2 atm, mixA: $N_2O(2\%)/H_2(1\%)/Ar(97\%)$, mixB: $N_2O(1\%)/ H_2(1\%)$ /Ar(98%) and mixC: $N_2O(1\%)/H_2(0.5\%)/$ Ar(98.5%). Symbols experimental data from [9], Lines model prediction from this work.

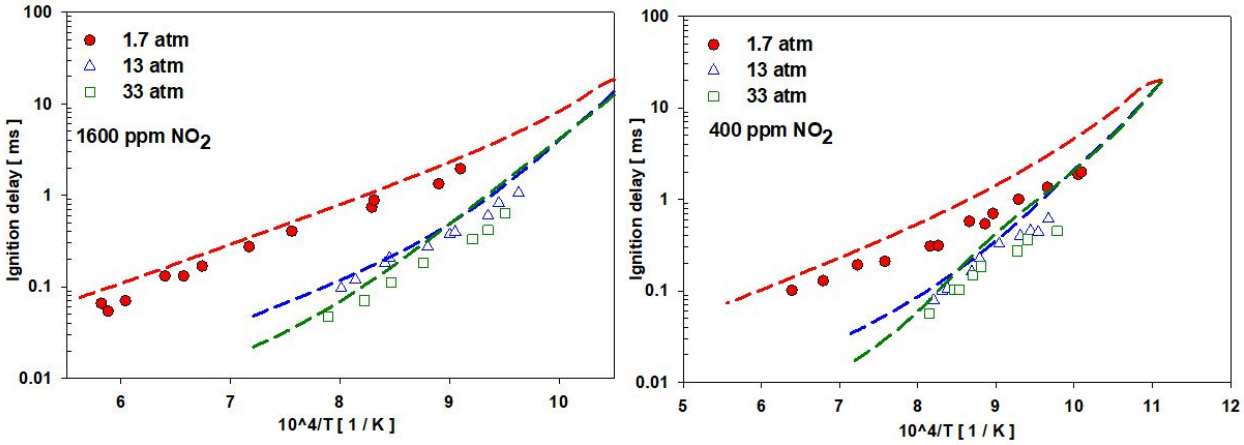

Figure S6: Ignition delay times comparison between model prediction and experimental data for $H_2/O_2/NO_2/Ar$ at varying NO_2 (400 ppm and 1600 ppm) concentration. Symbols: experimental data from [10]. Lines: prediction with current model.

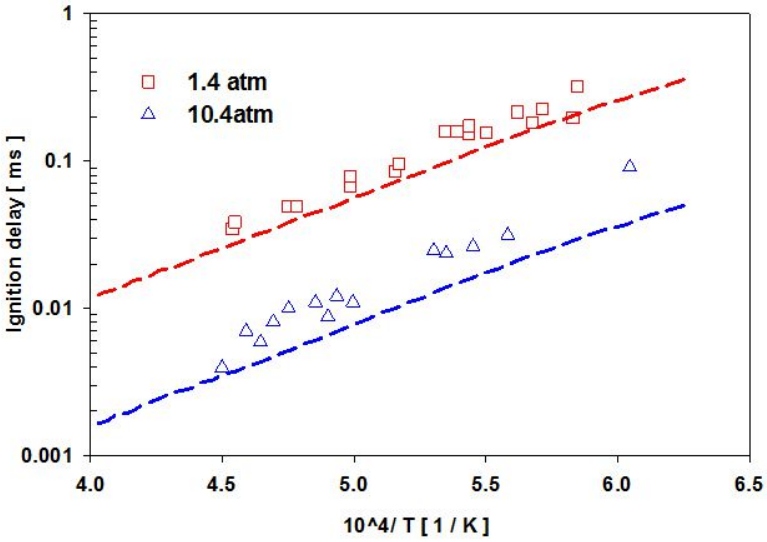

Figure S7: Ignition delay times comparison between model prediction and experimental data for H_2(0.0005)/CO(0.03)/N_2O(0.01)/Ar. Symbols: experimental data from [11]. Lines: prediction with current model.

2.3 Speciation in jet stirred reactor

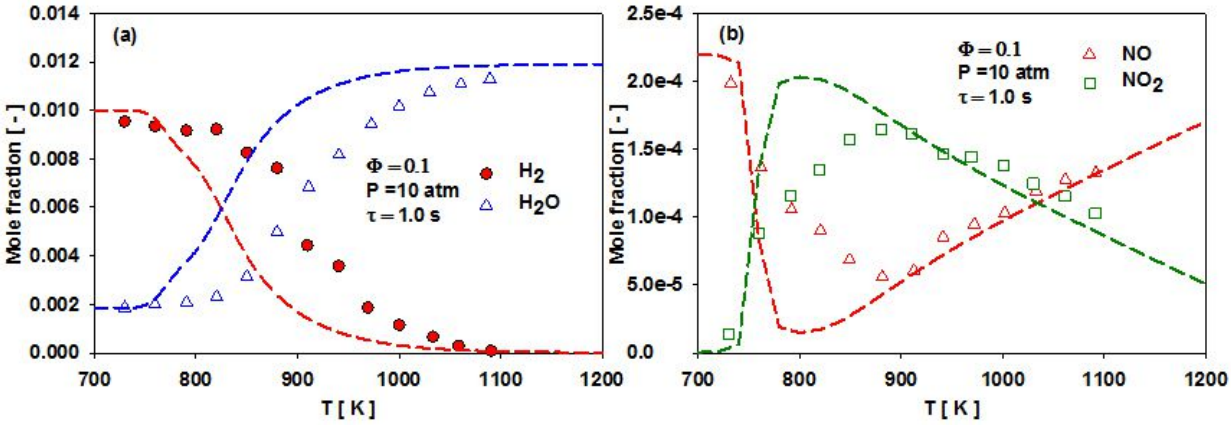

Figure S8: Species profile comparison between model prediction and experimental data for H_2 (0.01)/O_2/NO (220 ppm)/N_2 at 10 atm, ϕ = 0.1 and τ = 1.0 s in JSR. Symbols experimental data from [12], lines: model prediction from this work.

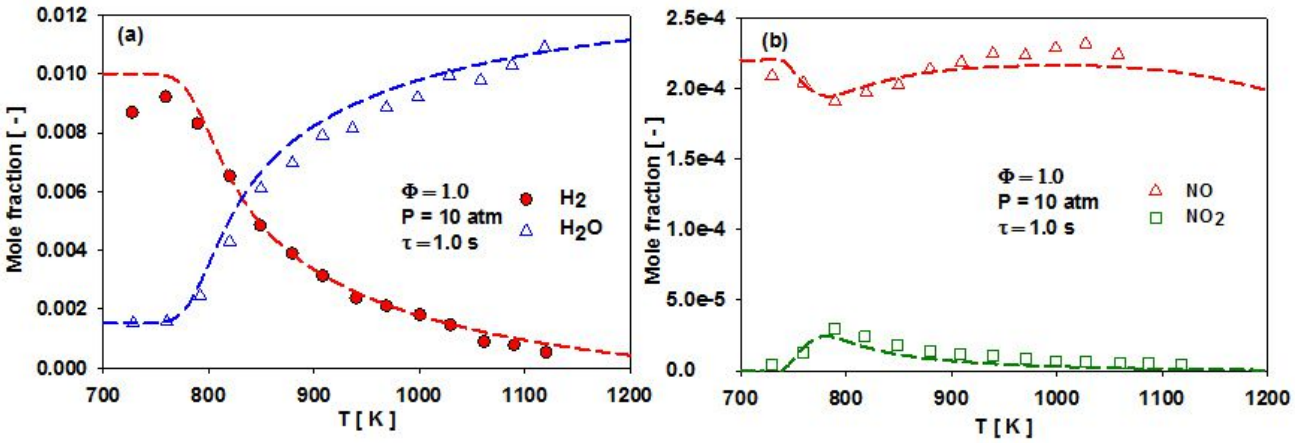

Figure S9: Species profile comparison between model prediction and experimental data for H_2 (0.01)/O_2/NO (220 ppm)/N_2 at 10 atm, ϕ = 1.0 and τ = 1.0 s in JSR. Symbols experimental data from [12], lines: model prediction from this work.

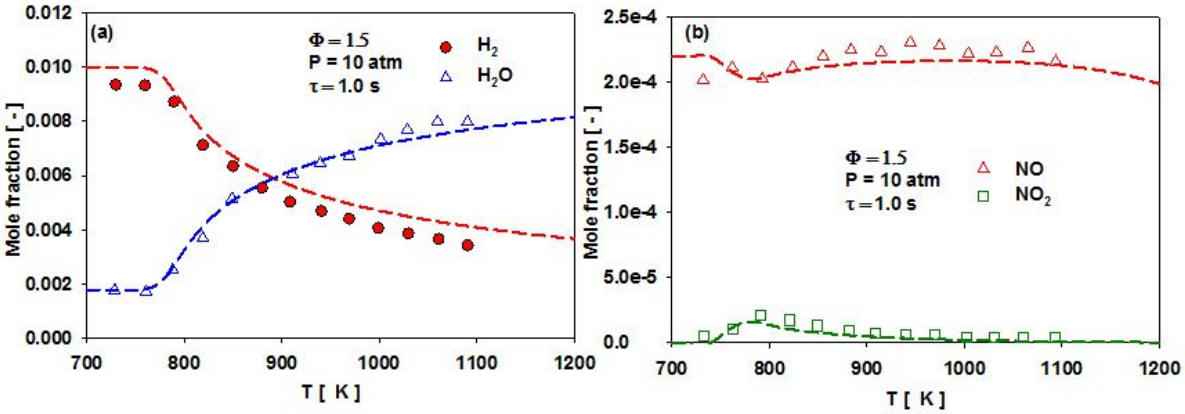

Figure S10: Species profile comparison between model prediction and experimental data for H_2 (0.01)/O_2/NO (220 ppm)/N_2 at 10 atm, ϕ = 1.5 and τ = 1.0 s in JSR. Symbols experimental data from [12], lines: model prediction from this work.

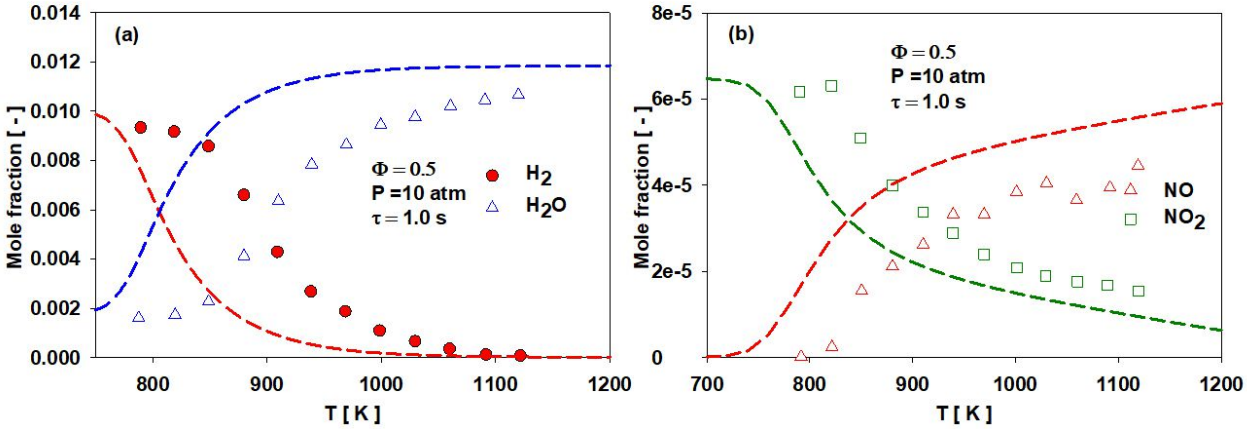

Figure S11: Species profile comparison between model prediction and experimental data for H_2 (0.01)/O_2/NO_2 (65 ppm)/N_2 at 10 atm, ϕ = 0.5 and τ = 1.0 s in JSR. Symbols experimental data from [12], lines: model prediction from this work.

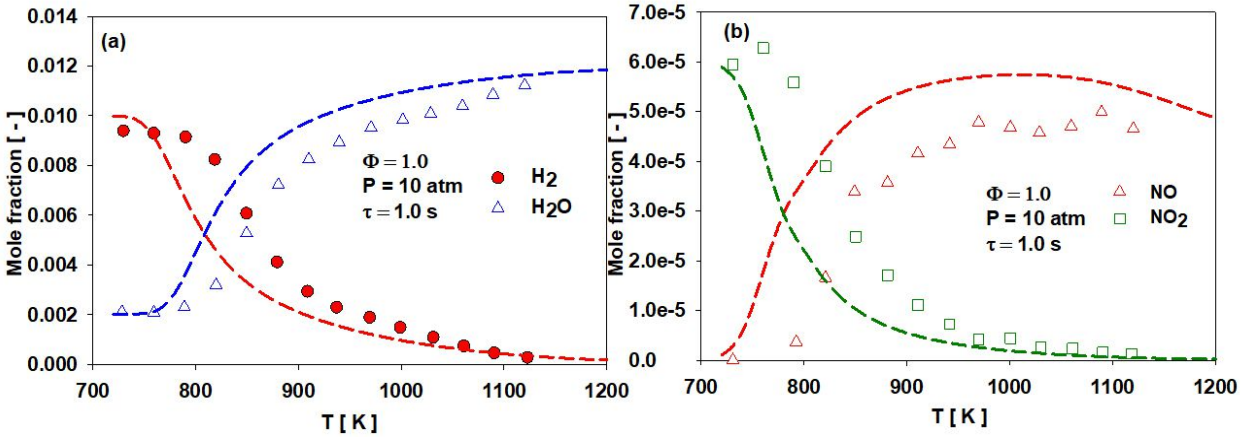

Figure S12: Species profile comparison between model prediction and experimental data for H_2 (0.01)/O_2/NO_2 (60 ppm)/N_2 at 10 atm, ϕ = 1.0 and τ = 1.0 s in JSR. Symbols experimental data from [12], lines: model prediction from this work.

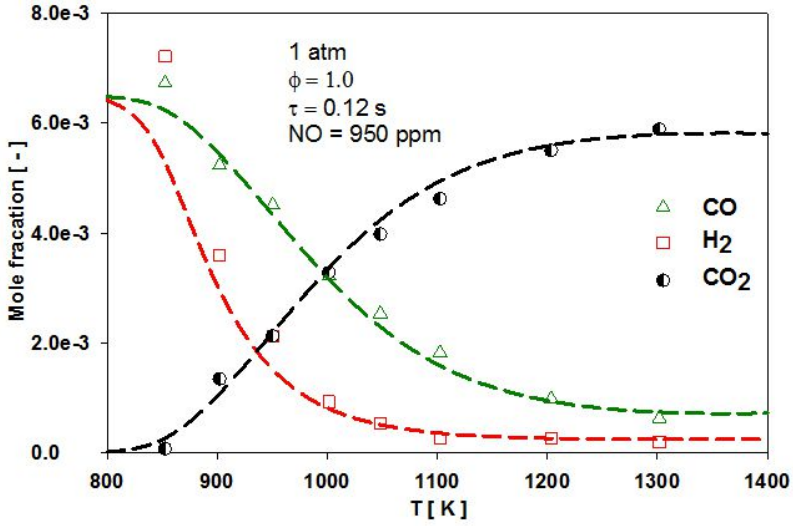

Figure S13: Species profile comparison between model prediction and experimental data for H_2/CO/NO (950 ppm)/O_2/N_2 at 1 atm, ϕ = 1.0 and τ = 0.12 s in JSR. Symbols experimental data from [13], lines: model prediction from this work.

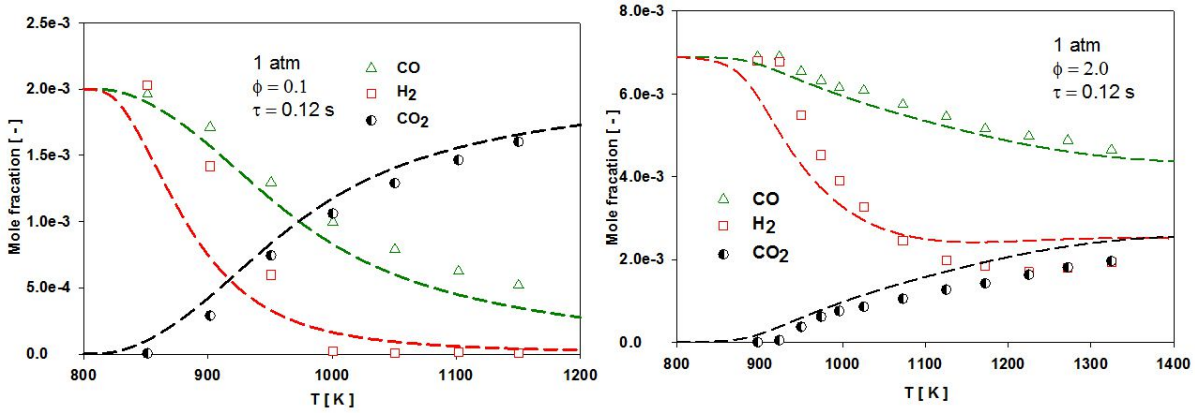

Figure S14: Figure S13: Species profile comparison between model prediction and experimental data for H_2/CO/NO (1000 ppm)/O_2/N_2 at 1 atm in JSR. Symbols experimental data from [13], lines: model prediction from this work.

2.4 Speciation in flow reactor

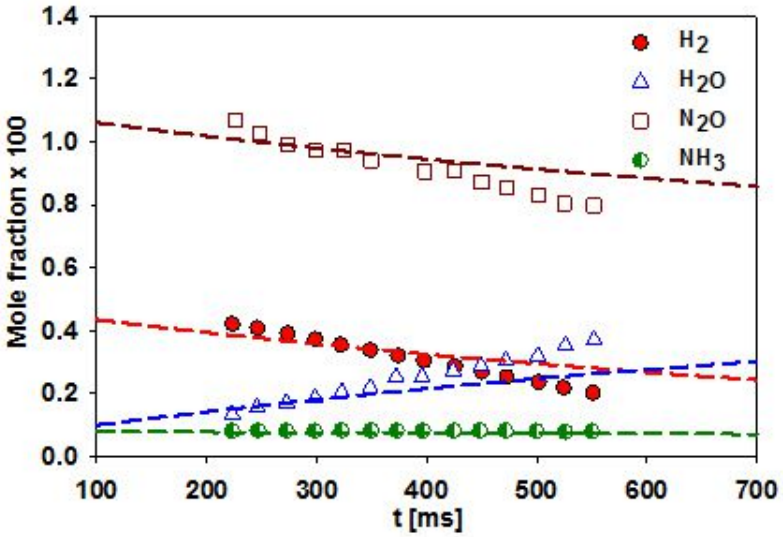

Figure S15: Species profile comparison between model prediction and experimental data for H_2 (0.53%)/N_2O (1.16%)/NH_3 (0.08%)/N_2 at 3atm and 995 K in flow reactor. Symbols experimental data from [14], lines: model prediction from this work. Simulation results are time shifted by 100 ms to match 50 % of the fuel consumption.

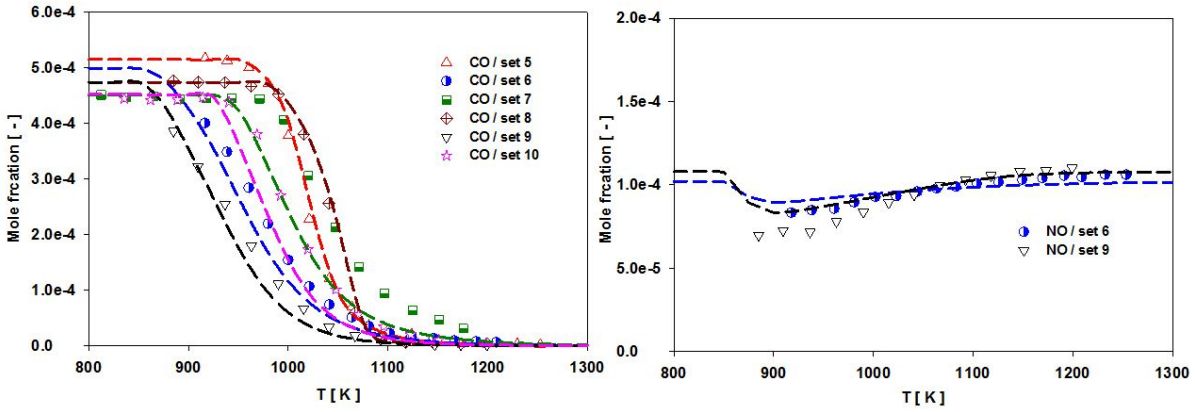

Figure S16: Speciation of CO/NO/O_2/H_2O/N_2 oxidation in flow reactor at 1.05 atm. Symbols: experimental data from [15]; lines: prediction with present model. Mixture number (or set no.) shown in legend are same in as [15].

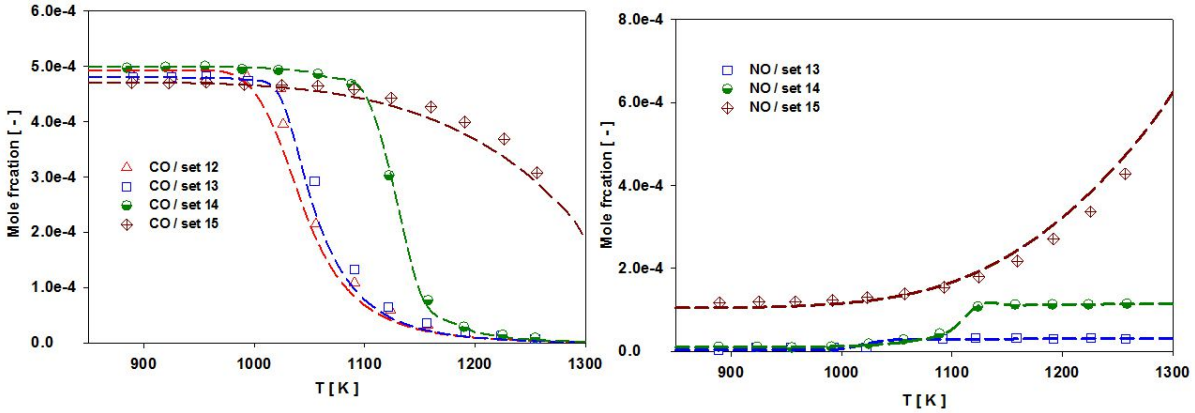

Figure S17: Speciation of $CO/NO/O_2/H_2O/N_2$ oxidation in flow reactor at 1.05 atm. Symbols: experimental data from [15]; lines: prediction with present model. Mixture number (or set no.) shown in legend are same as in[15].

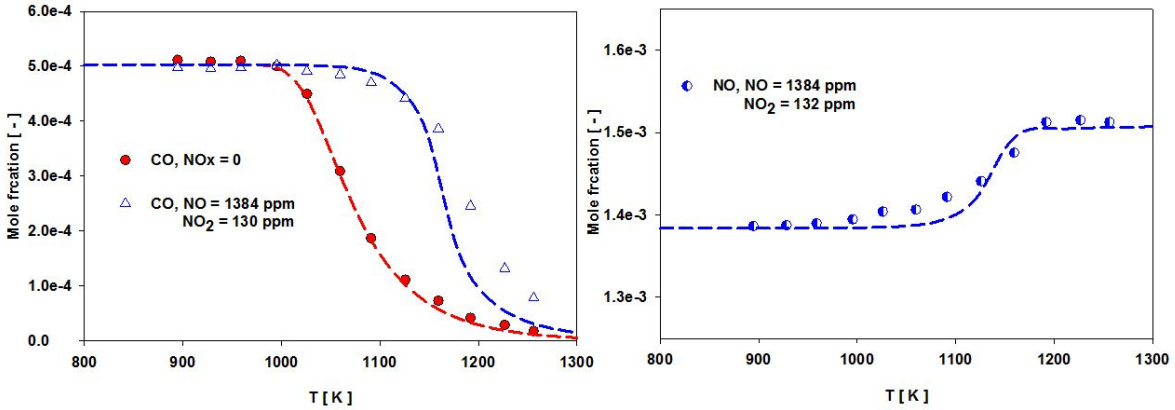

Figure S18: Speciation of $CO/NO/O_2/H_2O/N_2$ oxidation in flow reactor at 1.05 atm. Symbols: experimental data from [15]; lines: prediction with present model. $NO_x = 0$ ppm (set 16), $NO_x = 1514$ ppm (set 17) as in [15].

2.4 Speciation in burner stabilized flame

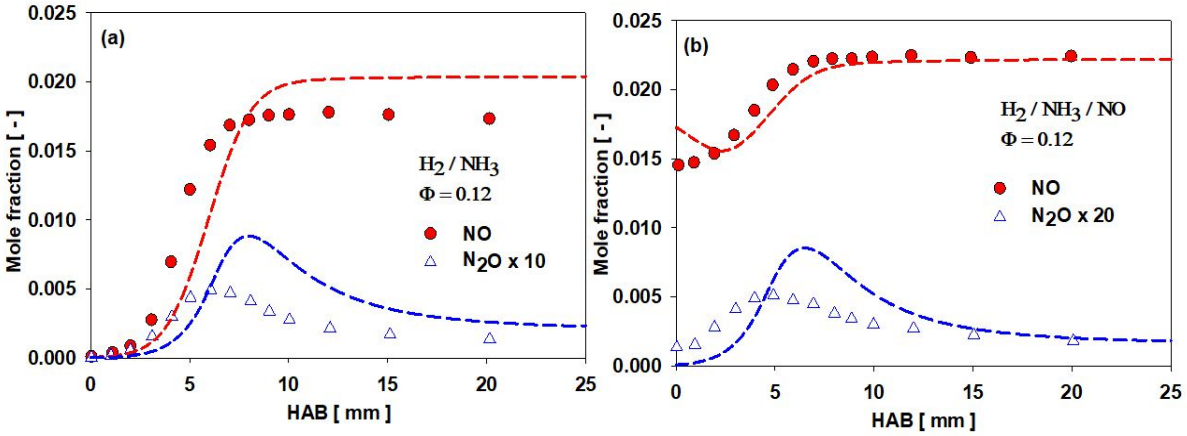

Figure S19: Species profile comparison between measurements and model prediction at 4.6 kPa (a), NH_3 (0.0340)/H_2 (0.1350)/O_2 (0.7650)/Ar; (b), NH_3 (0.017)/H_2 (0.1605)/NO (0.017)/O_2 (0.7565) /Ar premixed flame. Symbols: measurements from [16], lines: present model prediction.

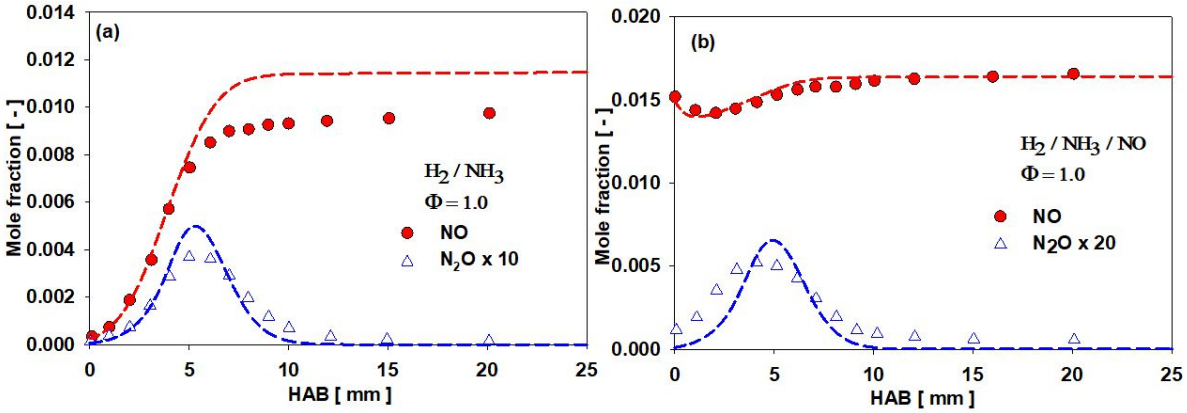

Figure S20: Species profile comparison between measurements and model prediction at 4.6 kPa (a) NH_3 (0.03)/H_2 (0.209)/O_2 (0.127)/Ar (0.634); (b) NH_3 (0.015)/H_2 (0.2315)/NO (0.015)/O_2 (0.1195)/Ar (0.6190) premixed flame. Symbols: measurements from [16], lines: present model prediction.

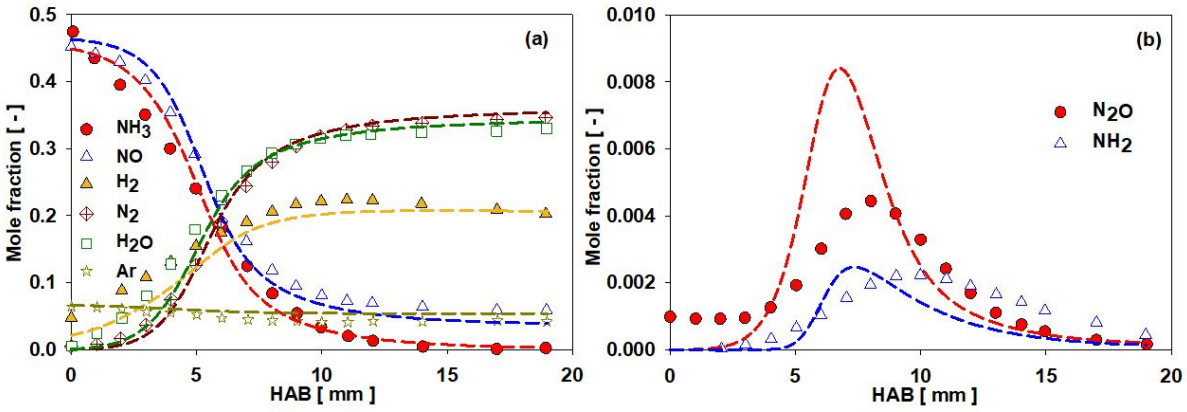

Figure S21: Species profile comparison between measurements and model prediction for NH_3 (0.461)/NO (0.472)/Ar (0.067) premixed flame at 7.2 kPa. Symbols: measurements from [17], lines: present model prediction.

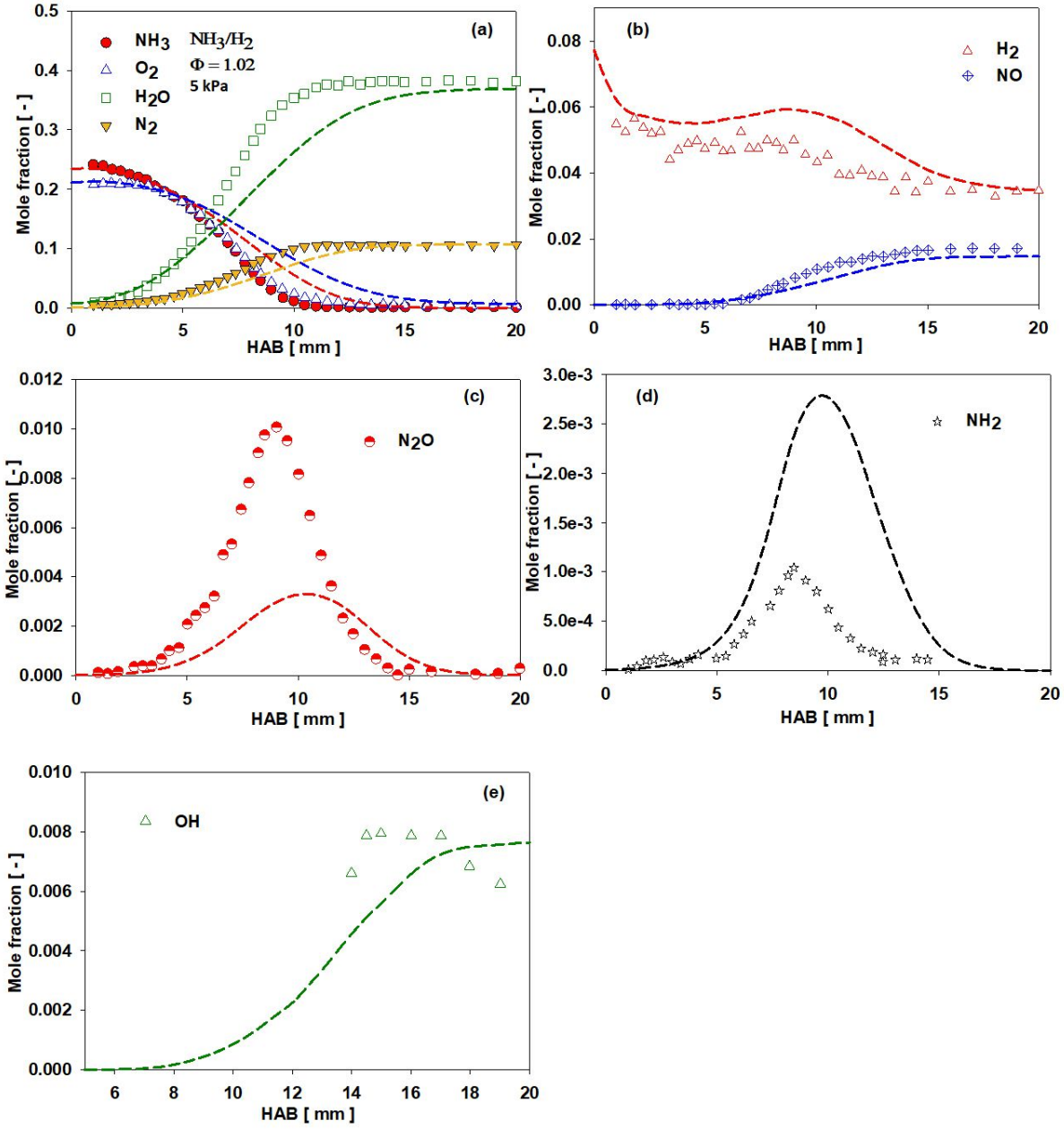

Figure S22: Species profile comparison between experimental data and model prediction. Symbols: experiments from [18], lines: present model prediction.

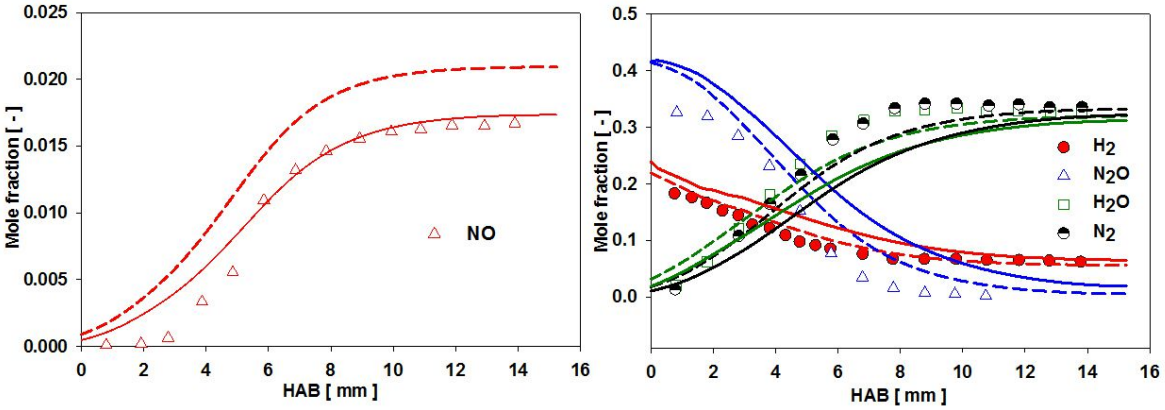

Figure S23: Species profile comparison between experimental data and model prediction for H_2/N_2O/Ar low pressure burner stabilized flame at 4.0 kPa. Symbols: experiments from [19] , lines: present model prediction.

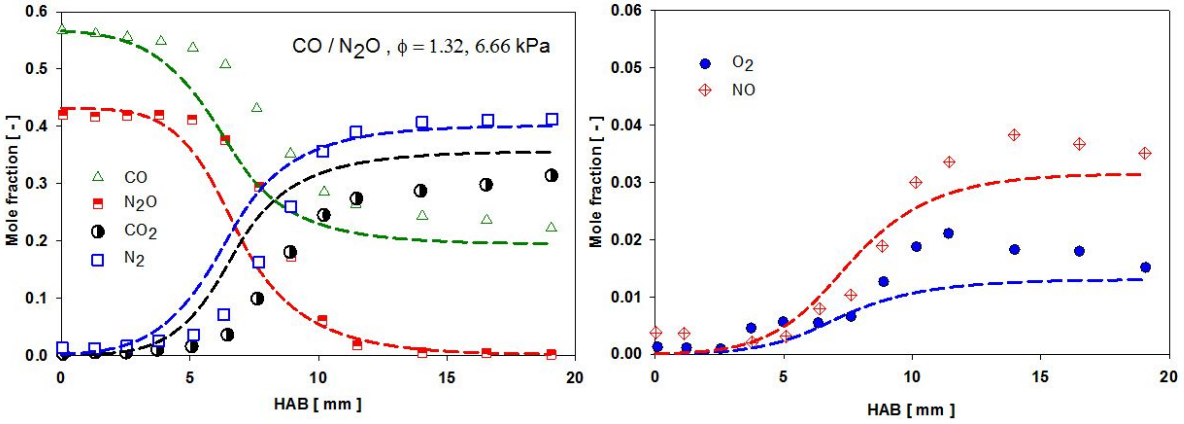

Figure S24: Species profile comparison between experimental data and model prediction for CO/N_2O low pressure burner stabilized flame at 6.66 kPa, ϕ = 1.32. Symbols: experiments from [20] , lines: present model prediction.

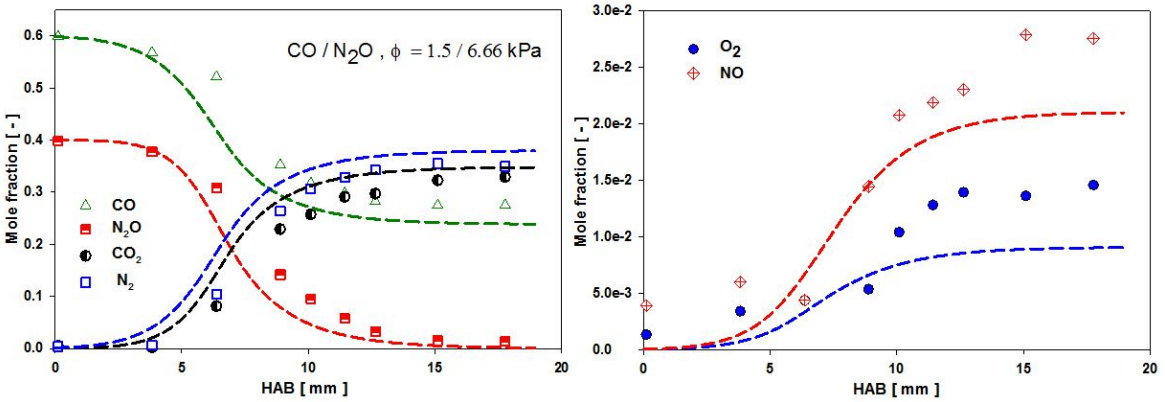

Figure S25: Species profile comparison between experimental data and model prediction for CO/N_2O low pressure burner stabilized flame at 6.66 kPa, ϕ = 1.50. Symbols: experiments from [20] , lines: present model prediction.

2.5 C_1/NO_x kinetic model validation

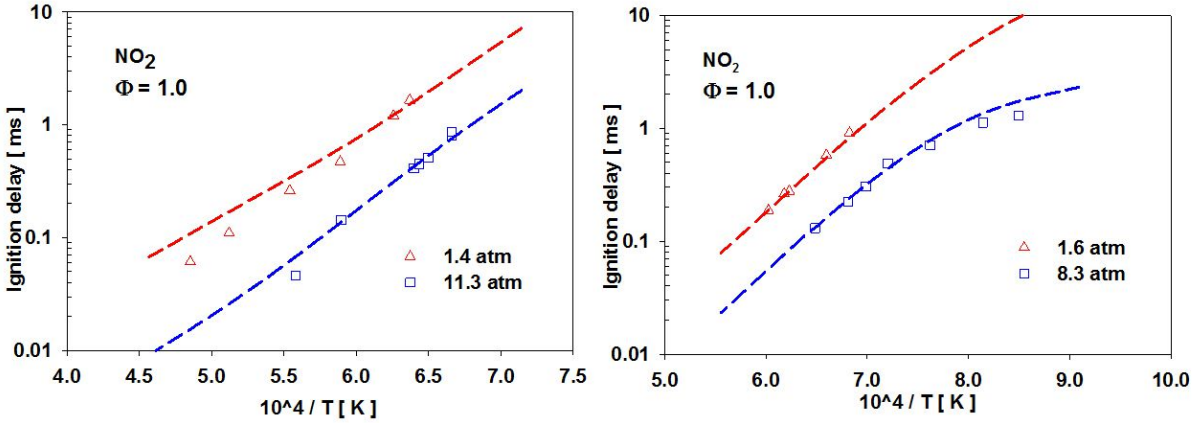

Figure S26: Ignition delay time comparison between model prediction and experimental data. Symbols: experimental data from [21], left (mix 7), right (mix 15) in their work, lines: present model prediction.

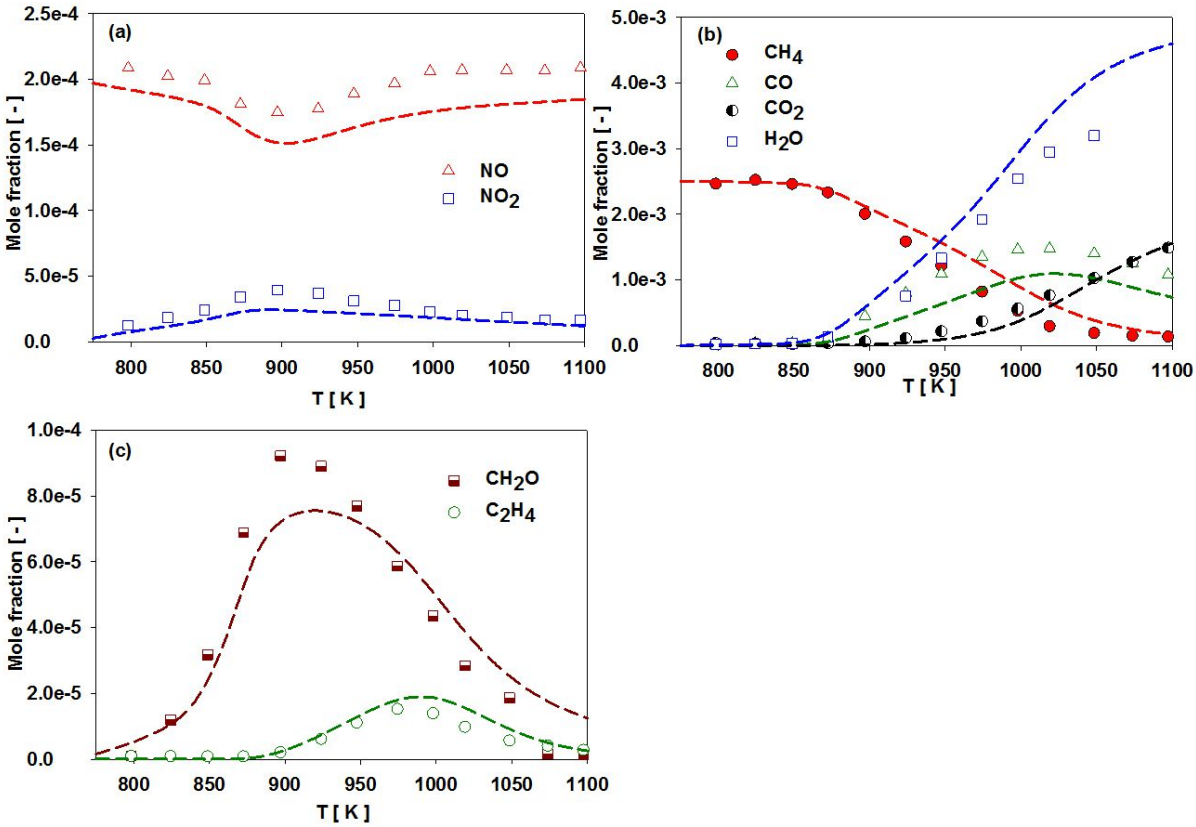

Figure S27: Species profile comparison between measurements and model prediction for CH_4 (0.25%)/O_2 (5%)/NO (0.02%)/N_2 oxidation in JSR at 1 atm, ϕ = 0.1and τ=0.12 s. Symbols: measurements from [22], lines: model prediction from this work.

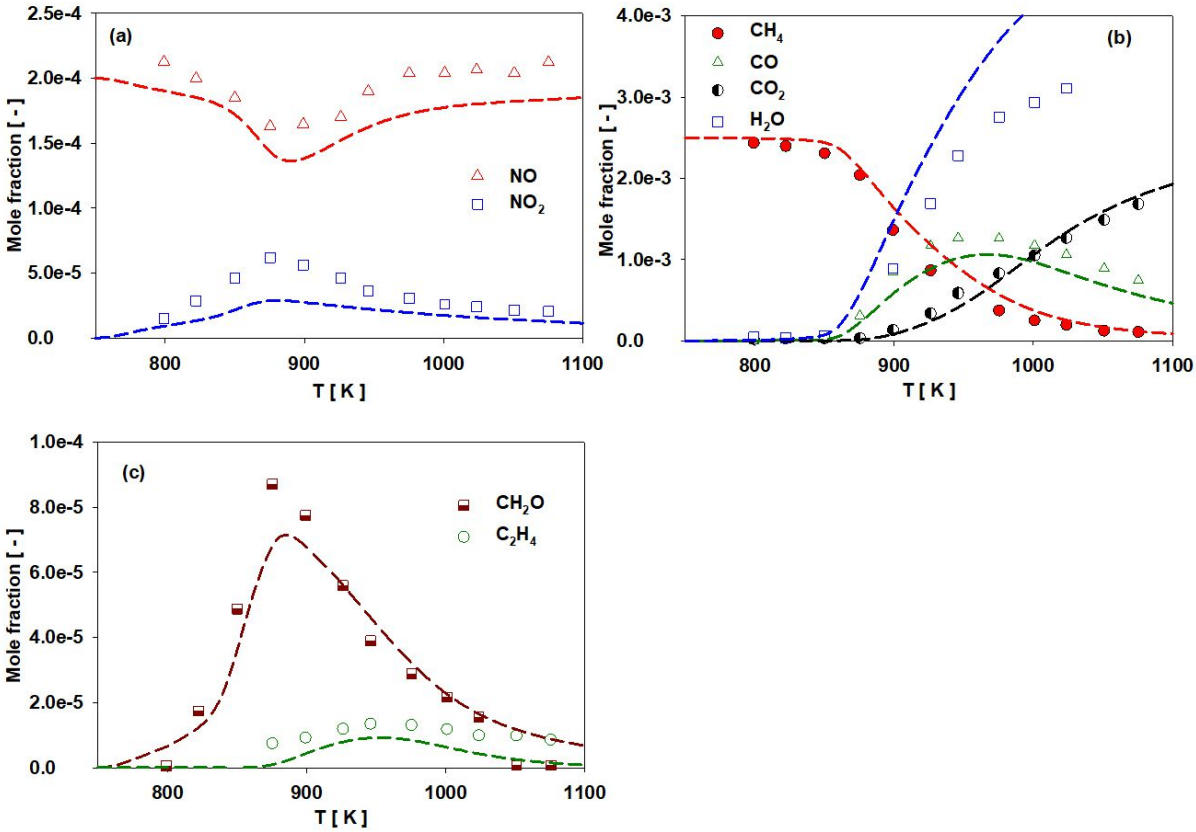

Figure S28: Species profile comparison between measurements and model prediction for CH_4 (0.25%)/ O_2 (5%)/ NO (0.02%)/N_2 oxidation in JSR at 1 atm, ϕ = 0.1and τ=0.24 s. Symbols: measurements from [22], lines: model prediction from this work.

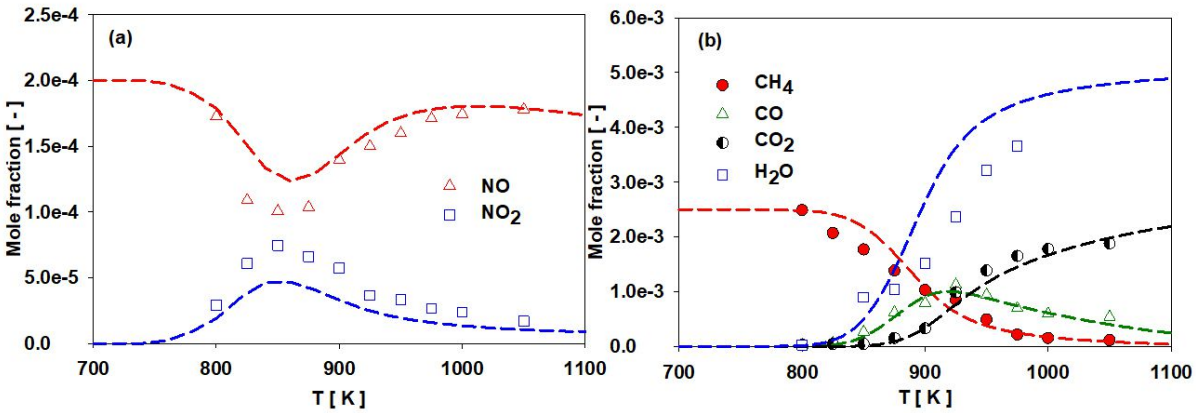

Figure S29: Species profile comparison between measurements and model prediction for CH_4 (0.25%)/ O_2 (1 %)/ NO (0.02%)/N_2 oxidation in JSR at 10 atm, ϕ = 0.5 and τ=1.0 s. Symbols: measurements from [22], lines: model prediction from this work.

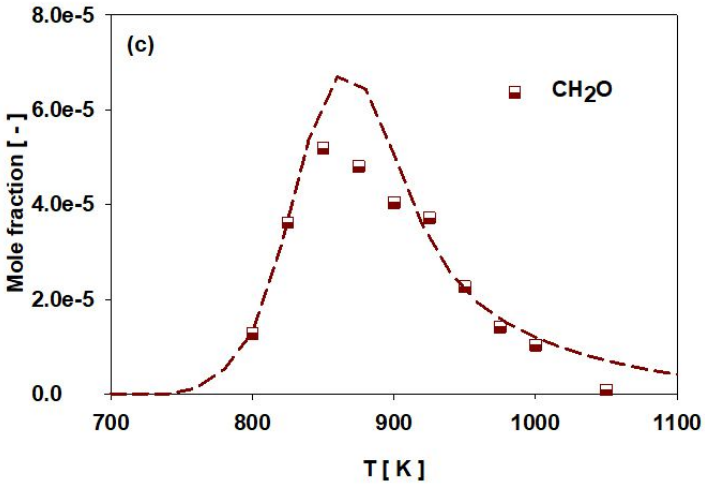

Figure S30: continuous of Figure S29

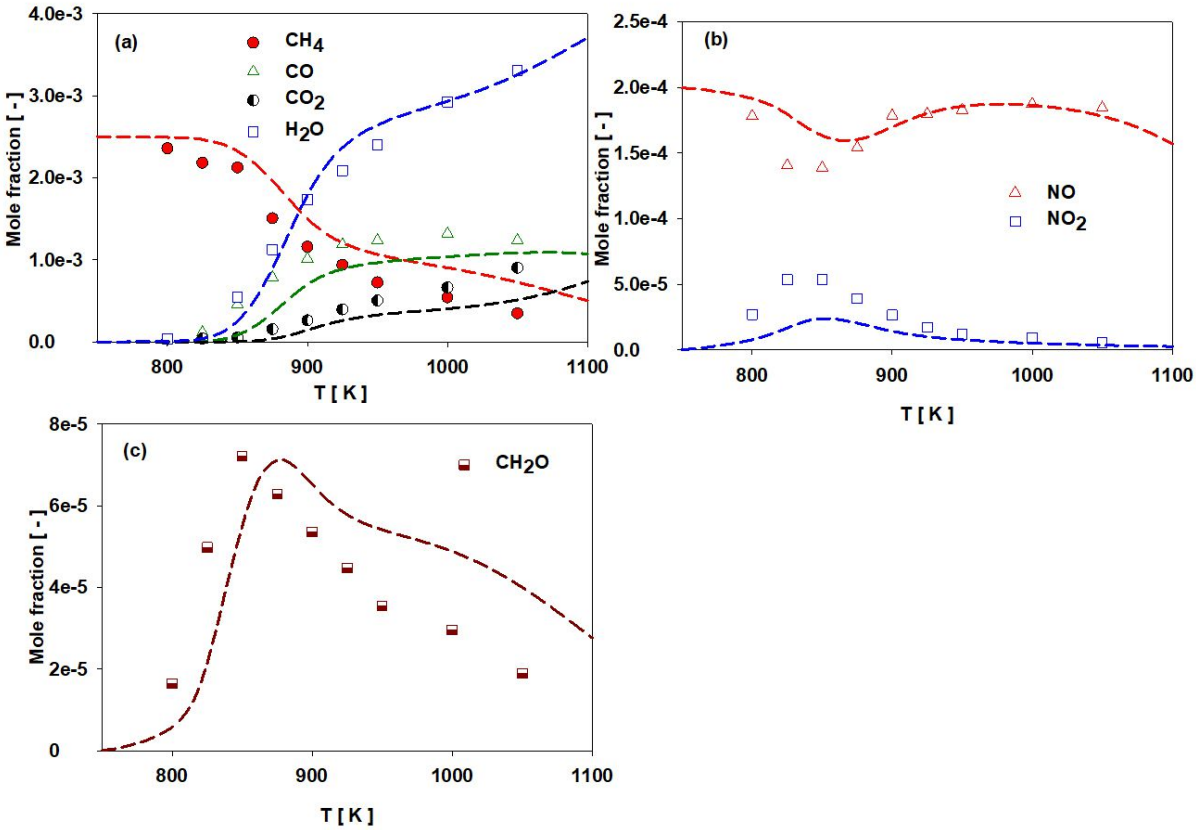

Figure S31: Species profile comparison between measurements and model prediction for CH_4 (0.25%)/ O_2 (0.5%)/ NO (0.02%)/N_2 oxidation in JSR at 10 atm, ϕ =1.0 and τ=1.0 s. Symbols: measurements from [22], lines: model prediction from this work.

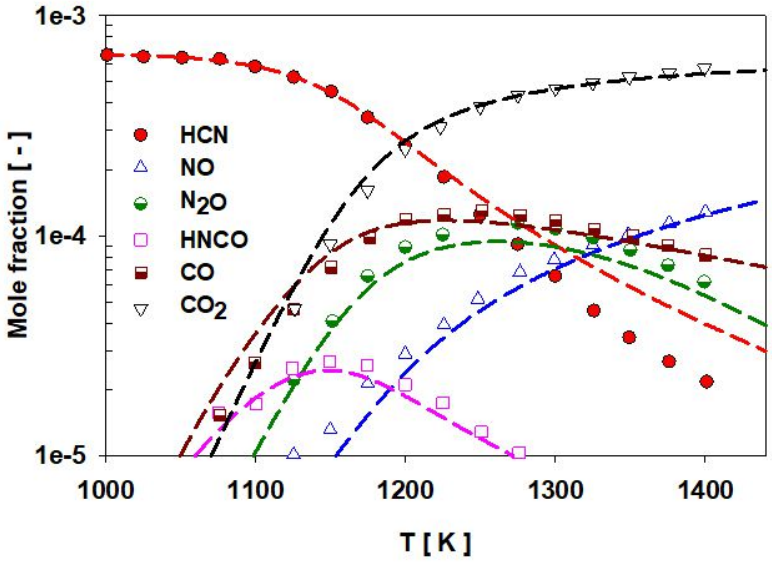

Figure S32: Species profile comparison between measurements and model prediction for HCN (0.067%)/ O_2 (0.2 %)/ H_2O (0.02%)/N_2 oxidation in JSR at 1 atm and τ=0.12 s. Symbols: measurements from [23], lines: model prediction from this work.

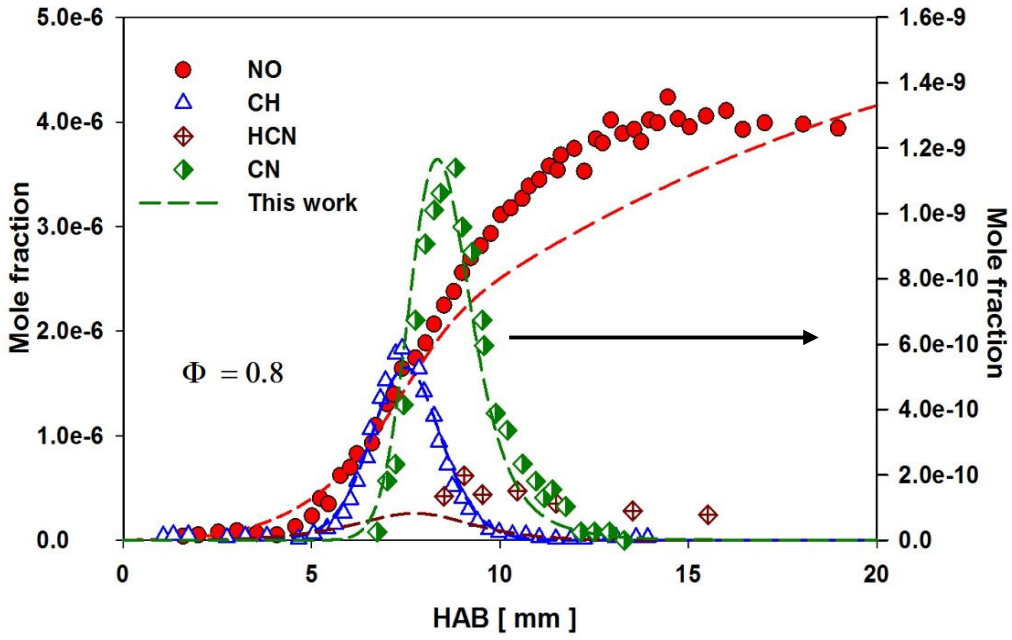

Figure S33: Speciation in premixed $CH_4/O_2/N_2$ flame at p = 5.3 kPa; T = 273.15 K; ϕ = 0.8. Symbols: measurements from Lamoureux et al. 2016 [24], present model prediction imposing experimental temperature profile. CN (Right axis).

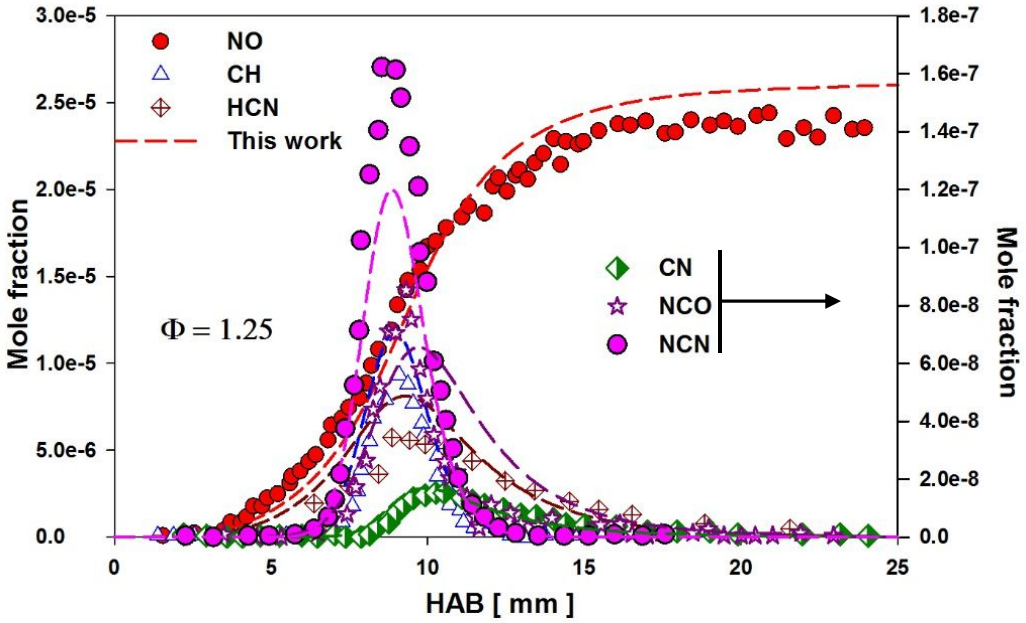

Figure S34: Speciation in premixed $CH_4/O_2/N_2$ flame at p = 5.3 kPa; T = 273.15 K; ϕ = 1.25. Symbols: measurements from Lamoureux et al. 2016 [24], lines: present model prediction imposing experimental temperature profile. CN (Right axis).

3. H_2/CO sub mechanism reaction rate comparison

3.1 Arrhenius Plots of Rate constant

The rate constant comparison of elementary reactions involved in H_2/CO system from different authors are shown below. The solid blue line represents the proposed rate constant by Baulch et.al. [25] whereas the blue dash line represents the lower uncertainty limit and blue dot line represents the upper uncertainty limit suggested by [25]. In the plots where Baulch et.al.[25] rate constant are not presented are the reactions that are not reviewed by them. The solid red line is the rate constant that is used in our work. Symbols represents the rate constant from other authors : Warnatz et.al.[26] (2006), cyan filled circle; Kéromnès et.al.[27] (2013), red filled triangle; Peters et.al.[28] (1993), pink filled square; NIST[29] , yellow filled square; San Diego (2014) [30], green filled square; Starik et.al.(2010) [31], black open square; Konnov (2008)[32], black half-

filled circle; Vagra et.al. (2016) [33], dark green open up triangle; Hong et.al. (2010, 2011, 2013)[34–36] dark red half-filled diamond, Mueller et.al. (1999) [37], dark yellow open down triangle; Burke et.al. (2012, 2013) [38,39], dark pink open star; Li et.al. (2015)[40], blue open star; Sun et.al. (2007) [41], red open up triangle; Li et.al. (2007) [42], dark red crossed square; Davis et.al. (2005) [43], blue open circle; Troe (2011) [44], red plus. Reaction rate constant from different authors which are presented in Arrhenius plots can be found in kinetic scheme.

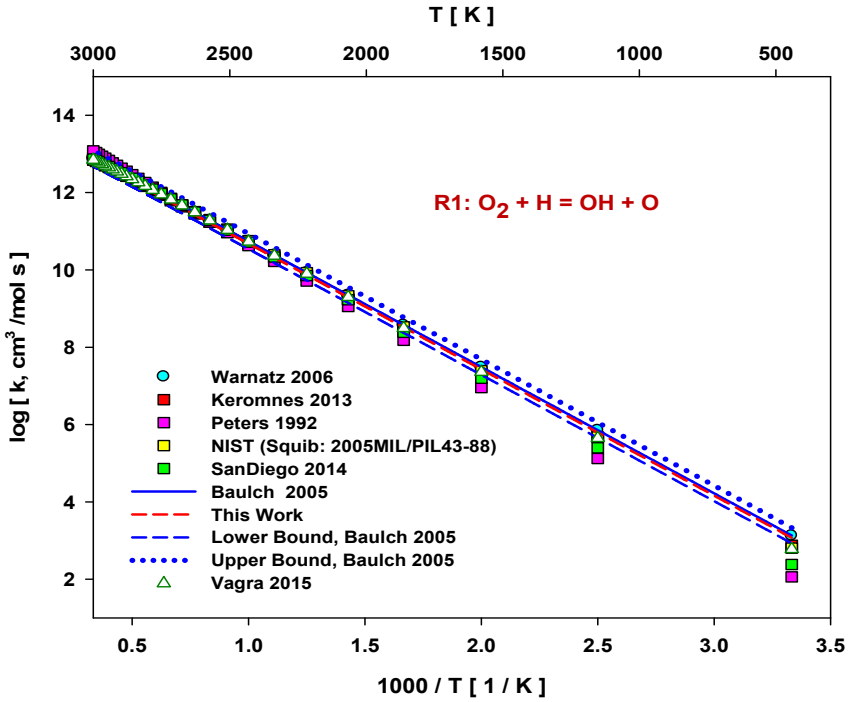

Figure S3.1: Rate constant comparison of reaction R1: O_2+H=OH+O from different authors.

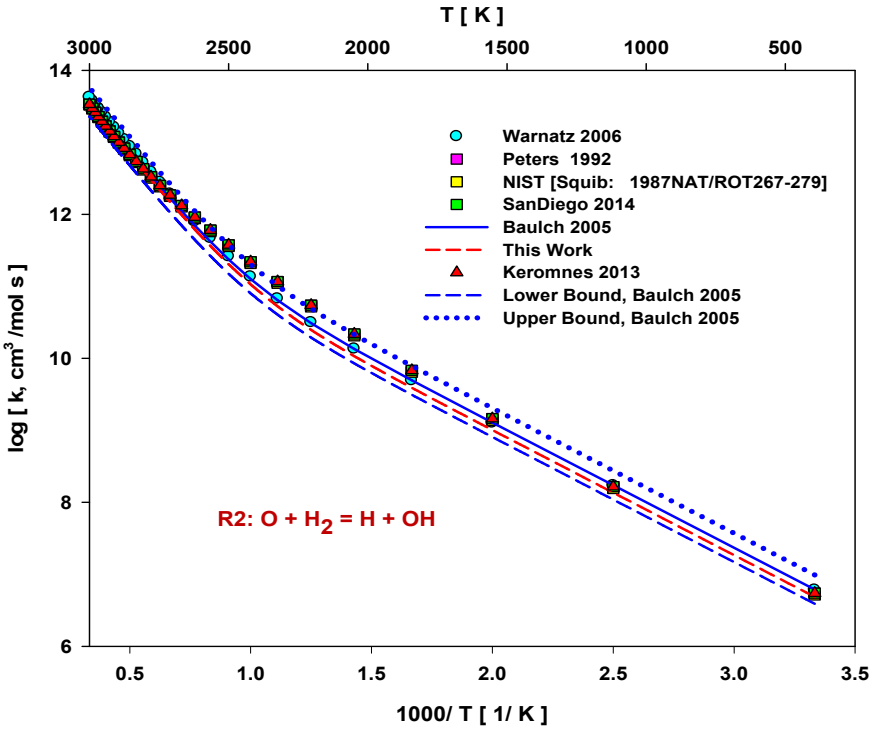

Figure S3.2: Rate constant comparison of reaction R2: O+H_2=H+OH from different authors.

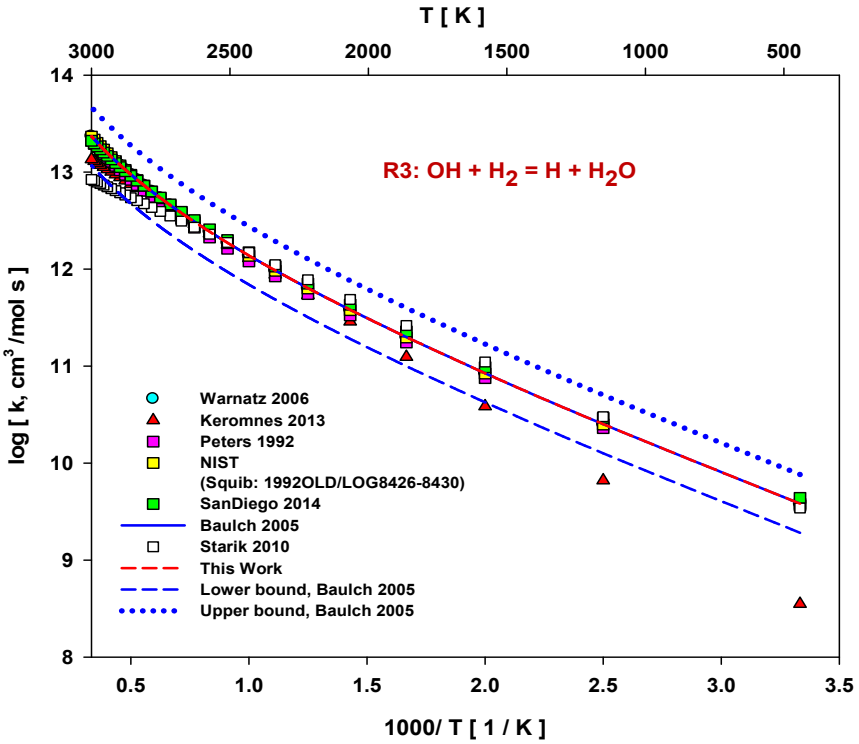

Figure S3.3: Rate constant comparison of reaction R3: OH+H_2=H+H_2O from different authors.

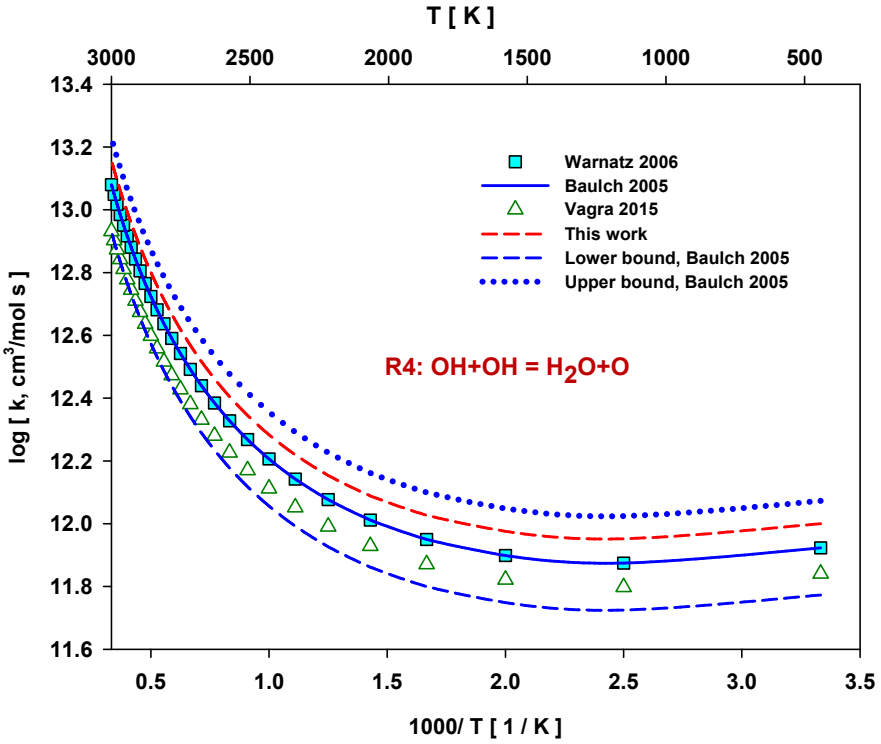

Figure S3.4: Rate constant comparison of reaction R4: OH+OH=H_2O+O from different authors.

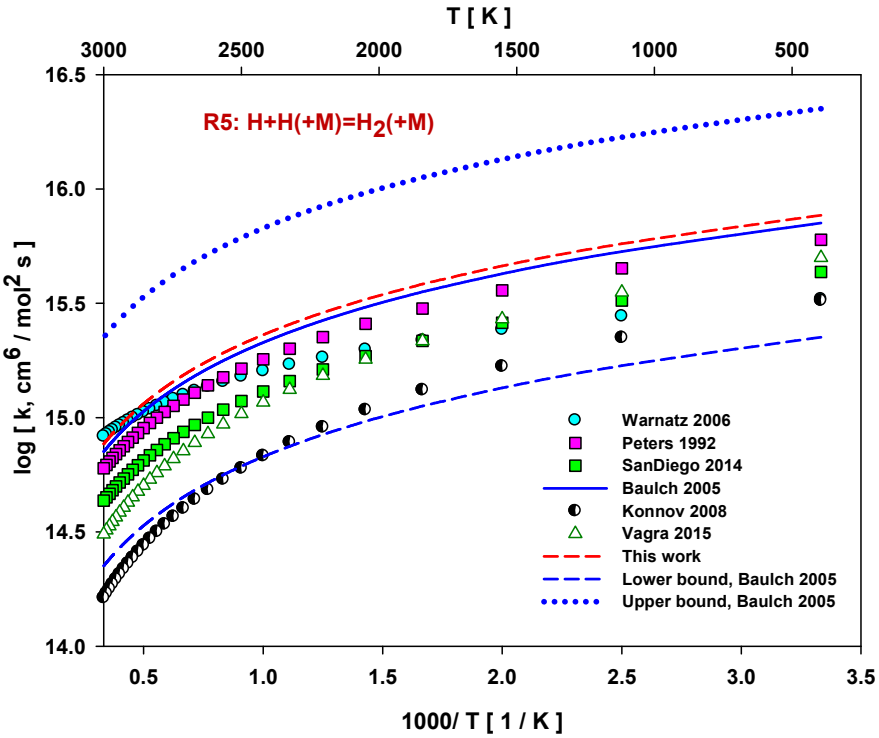

Figure S3.5: Rate constant comparison of reaction R5: H+H (+M) =H_2 (+M) from different authors.

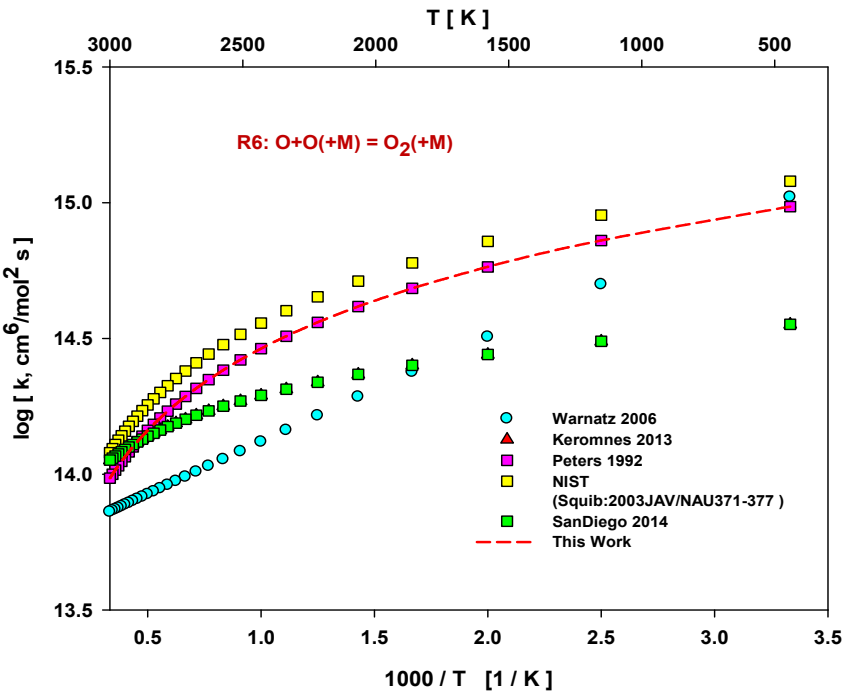

Figure S3.6: Rate constant comparison of reaction R6: O+O (+M) =O_2 (+M) from different authors.

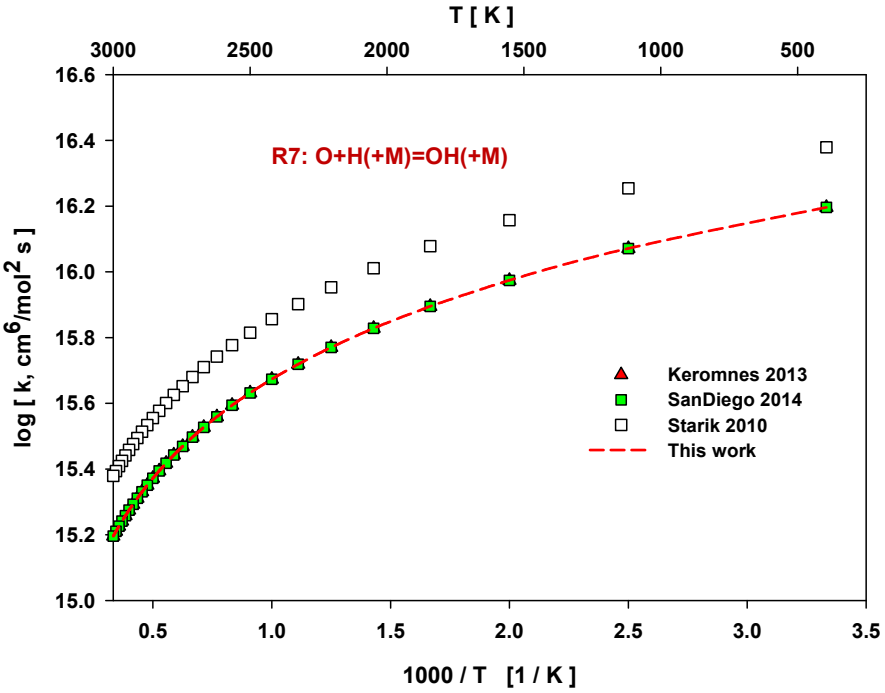

Figure S3.7: Rate constant comparison of reaction R7: O+H (+M) =OH (+M) from different authors.

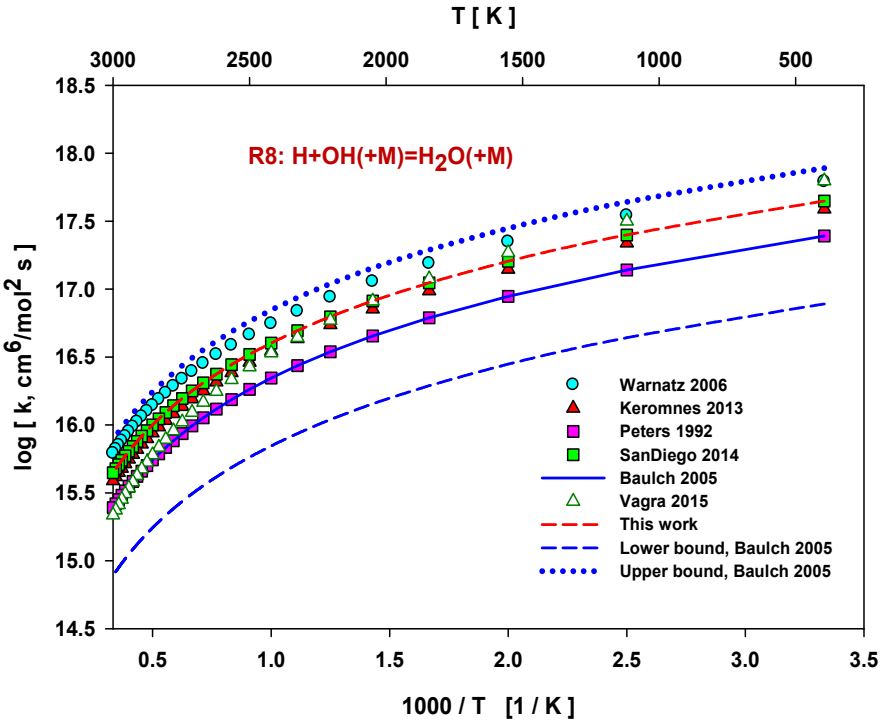

Figure S3.8: Rate constant comparison of reaction R8: H+OH (+M) =H_2O (+M) from different authors.

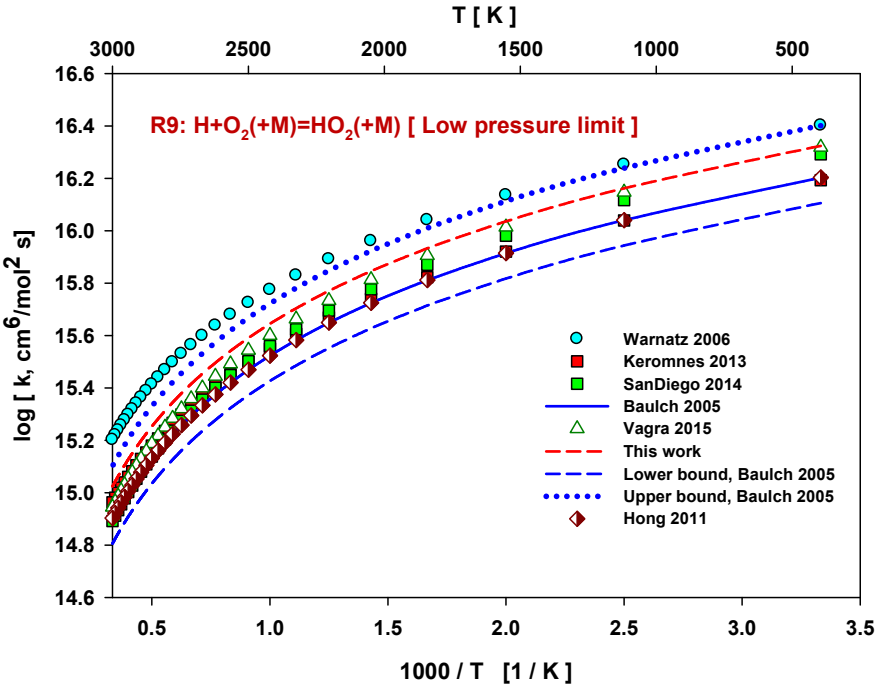

Figure S3.9: Rate constant comparison of reaction R9: H+O_2 (+M) =HO_2 (+M) from different authors.

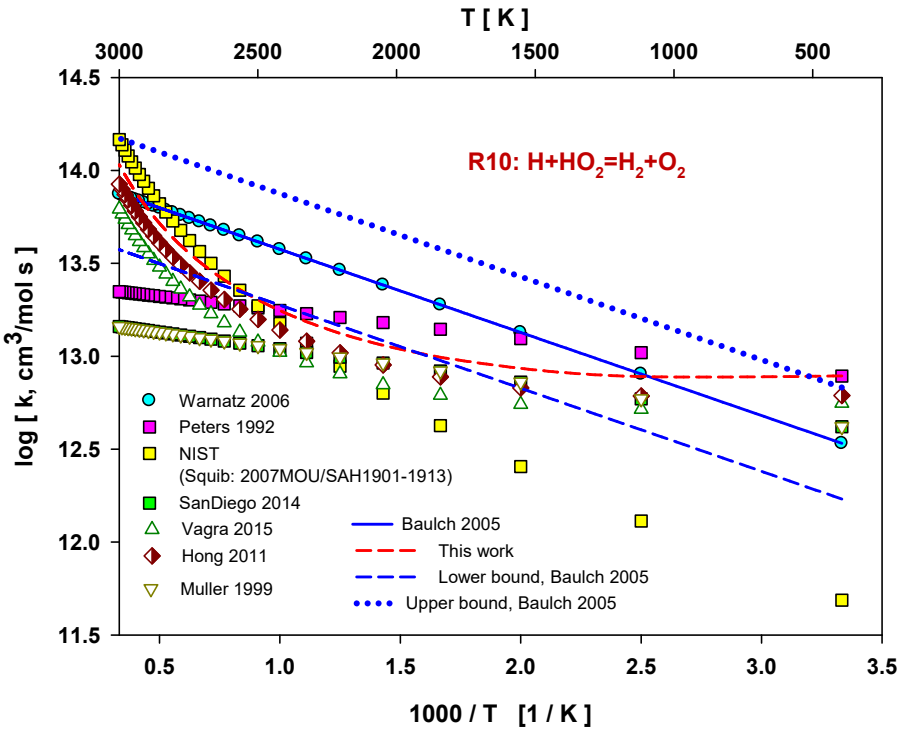

Figure S3.10: Rate constant comparison of reaction R10: $H+HO_2 = H_2+O_2$ from different authors.

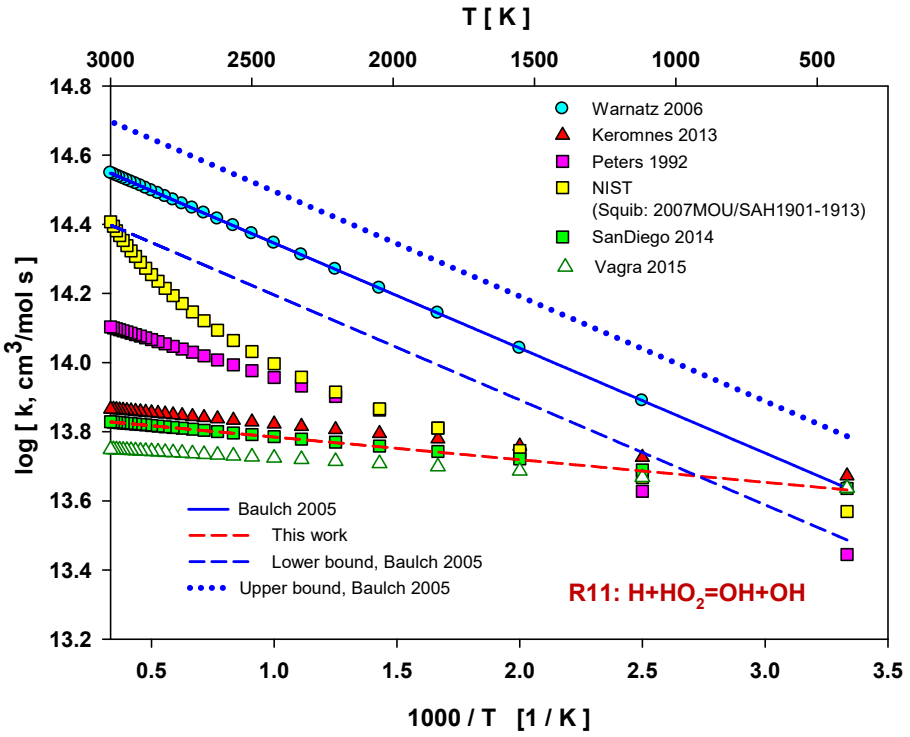

Figure S3.11: Rate constant comparison of reaction R11: $H+HO_2 =OH+OH$ from different authors.

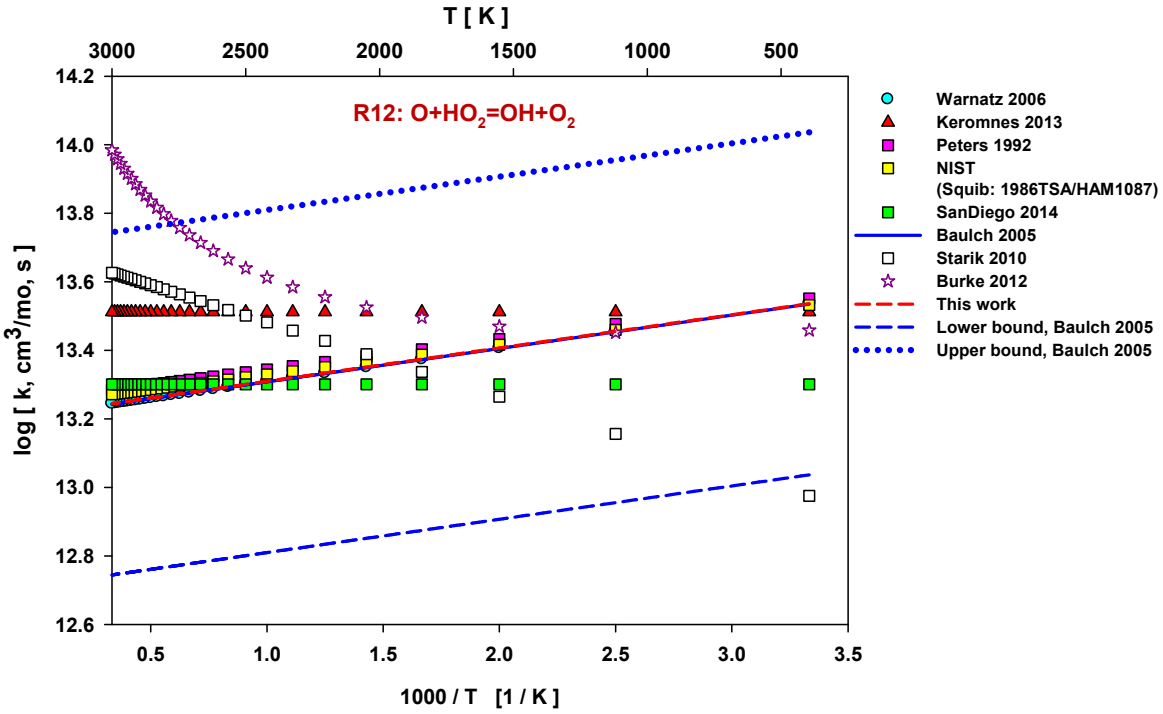

Figure S3.12: Rate constant comparison of reaction R12: $O+HO_2 =OH+O_2$ from different authors.

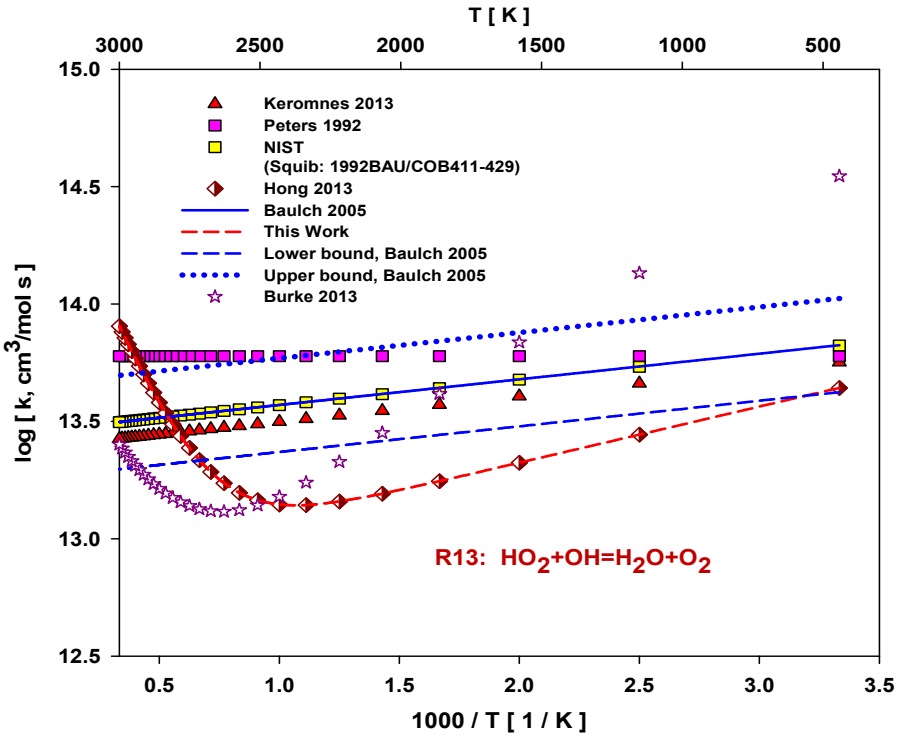

Figure S3.13: Rate constant comparison of reaction R13: $HO_2+OH=H_2O+O_2$ from different authors.

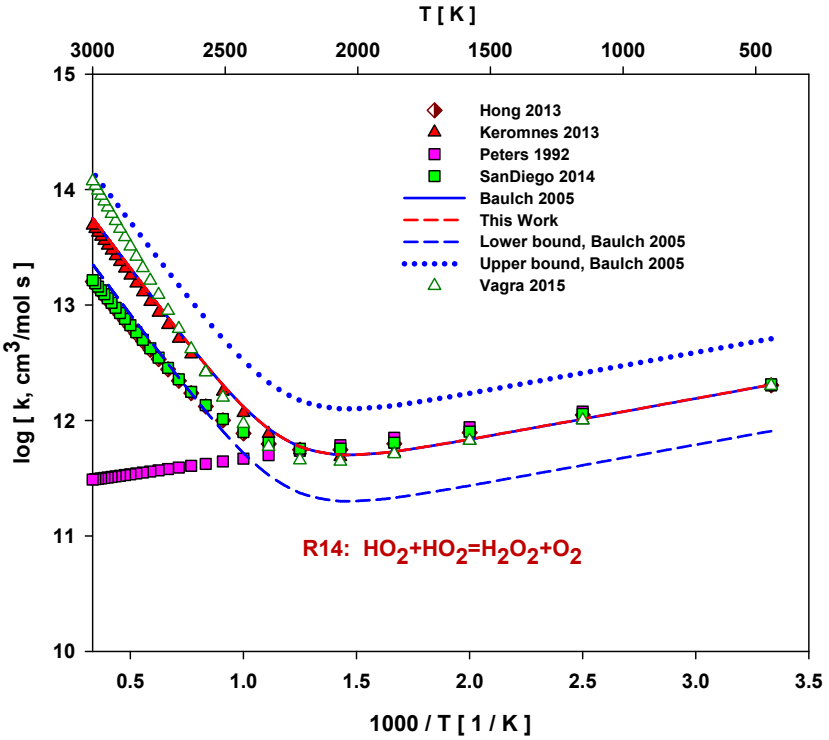

Figure S3.14: Rate constant comparison of reaction R14: HO_2+ HO_2=H_2O_2+O_2 from different authors.

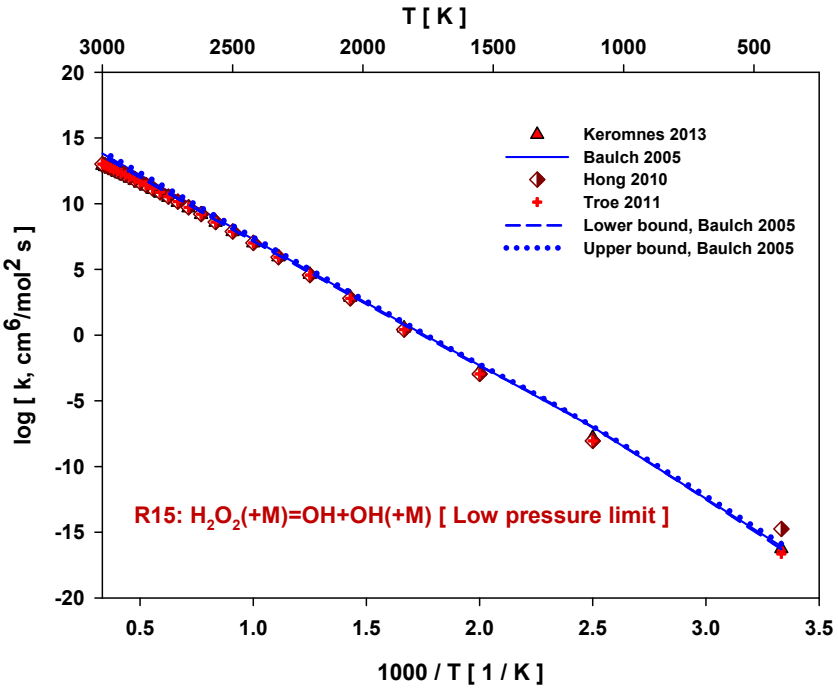

Figure S3.15: Rate constant comparison of reaction R15: H_2O_2 (+M) =OH+OH from different authors.

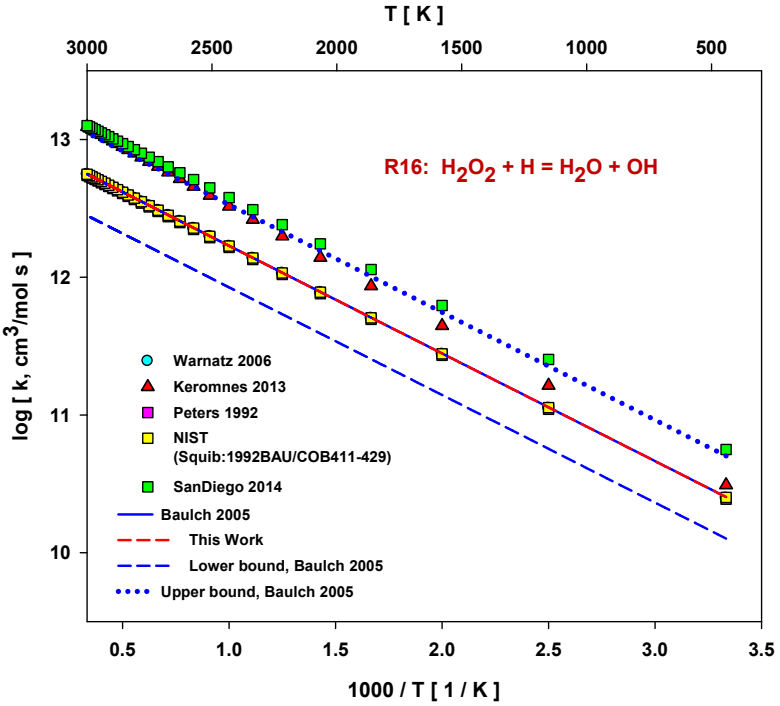

Figure S3.16: Rate constant comparison of reaction R16: $H_2O_2+H = H_2O+OH$ from different authors.

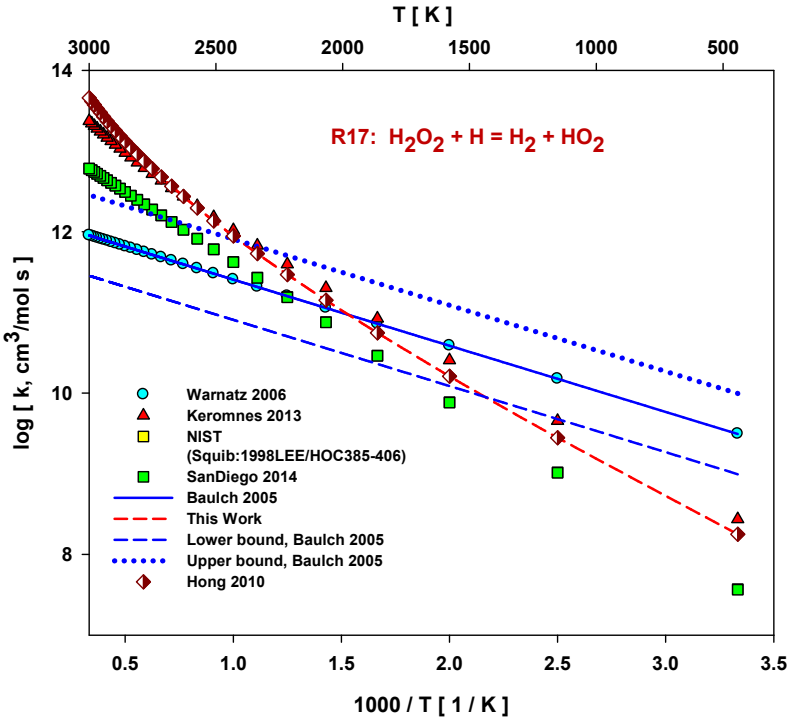

Figure S3.17: Rate constant comparison of reaction R17: $H_2O_2+H = H_2+HO_2$ from different authors.

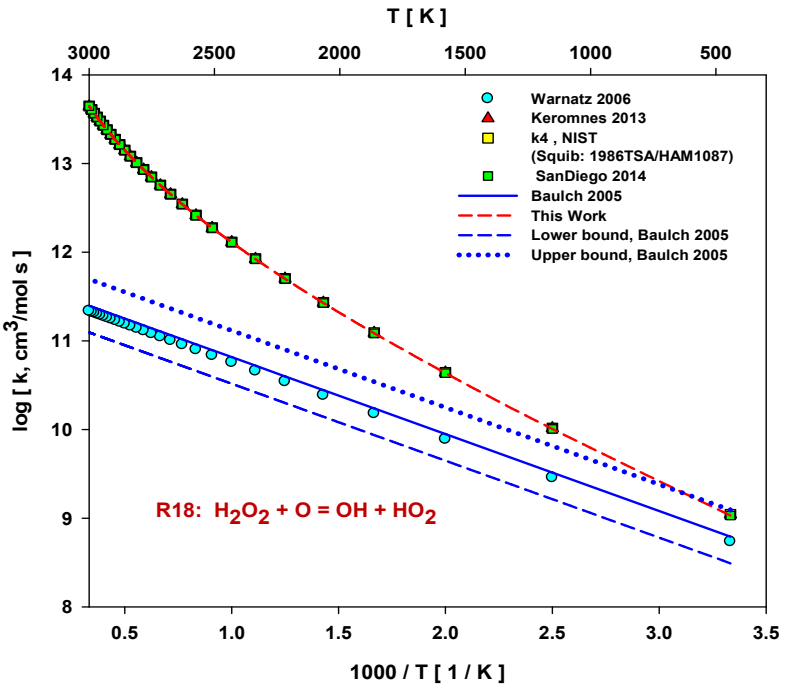

Figure S3.18: Rate constant comparison of reaction R18: H_2O_2+O =OH+HO_2 from different authors.

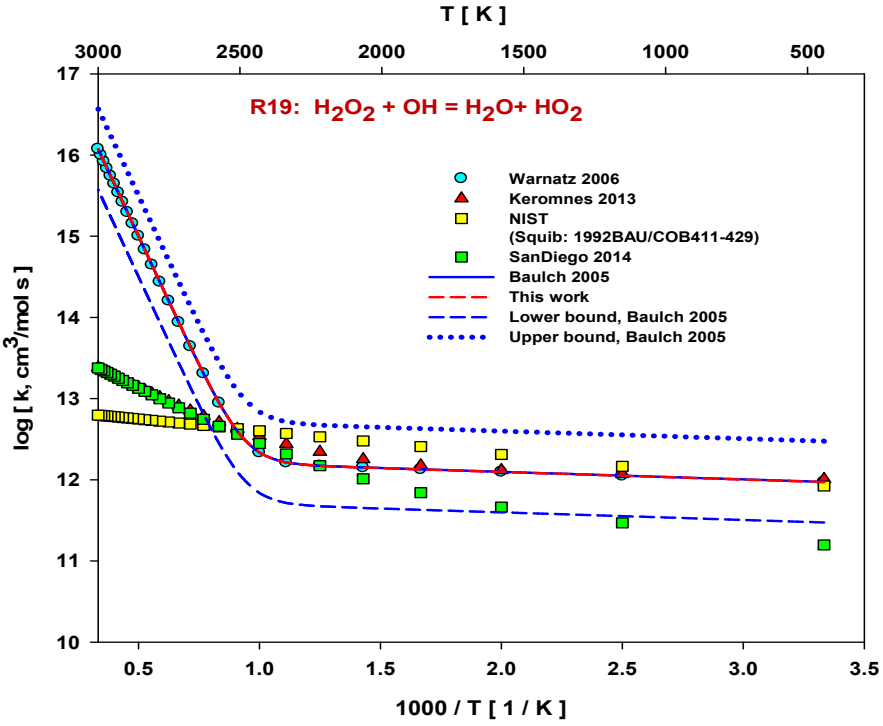

Figure S3.19: Rate constant comparison of reaction R19: H_2O_2+OH =H_2O+HO_2 from different authors.

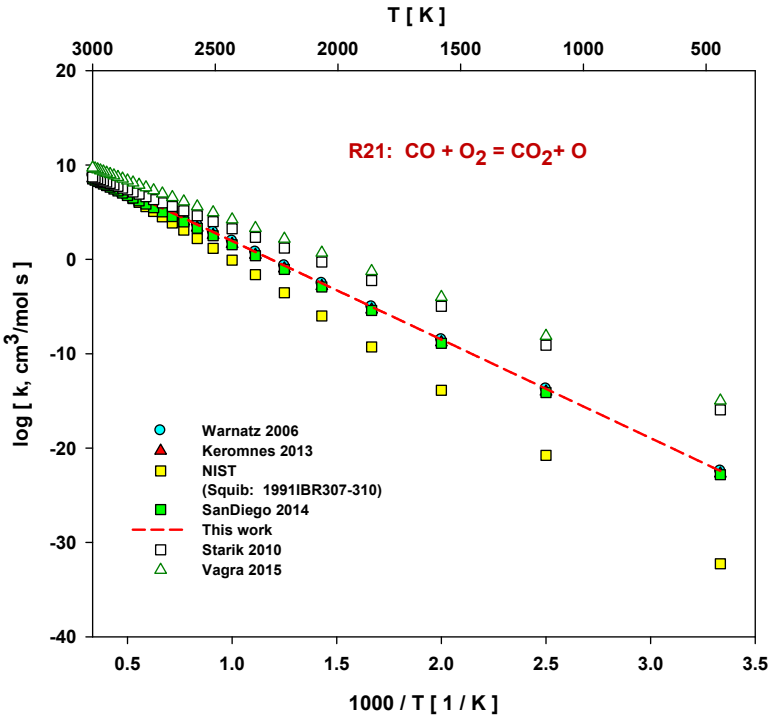

Figure S3.20: Rate constant comparison of reaction R21: $CO+O_2 = CO_2+O$ from different authors.

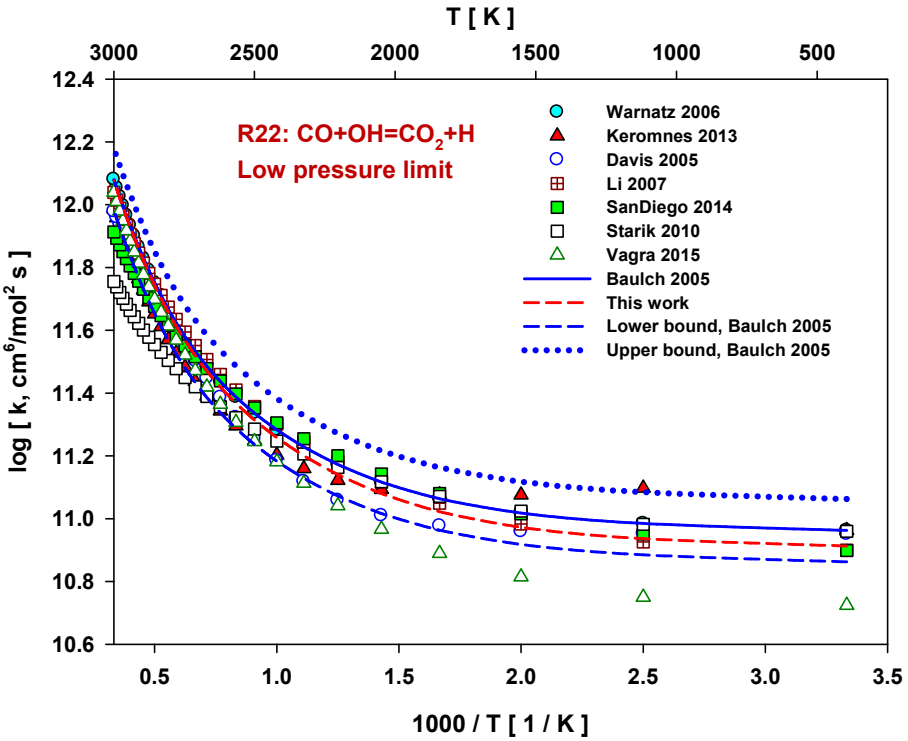

Figure S3.21: Rate constant comparison of reaction R22: $CO+OH = CO_2+H$ from different authors.

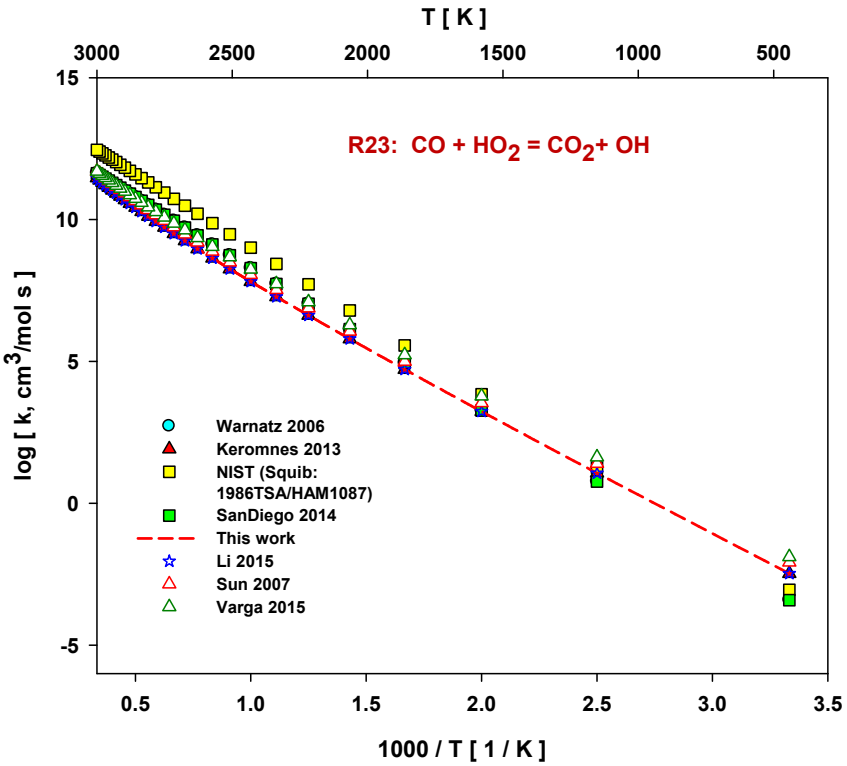

Figure S3.22: Rate constant comparison of reaction R23: $CO+HO_2 = CO_2+OH$ from different authors.

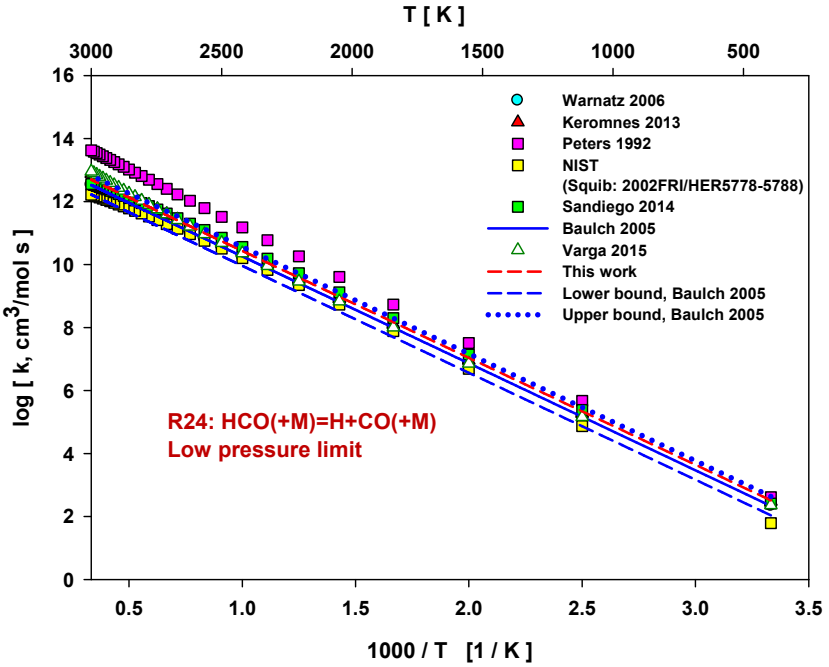

Figure S3.23: Rate constant comparison of reaction R24: HCO (+M) =H+CO (+M) from different authors.

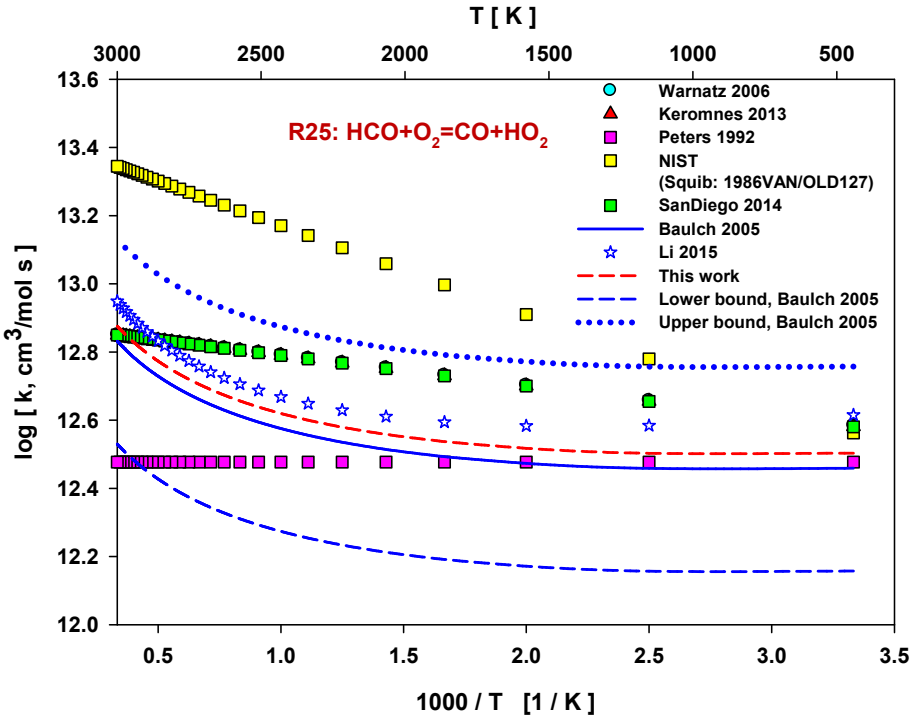

Figure S3.24: Rate constant comparison of reaction R25: $HCO+O_2 = CO+HO_2$ from different authors.

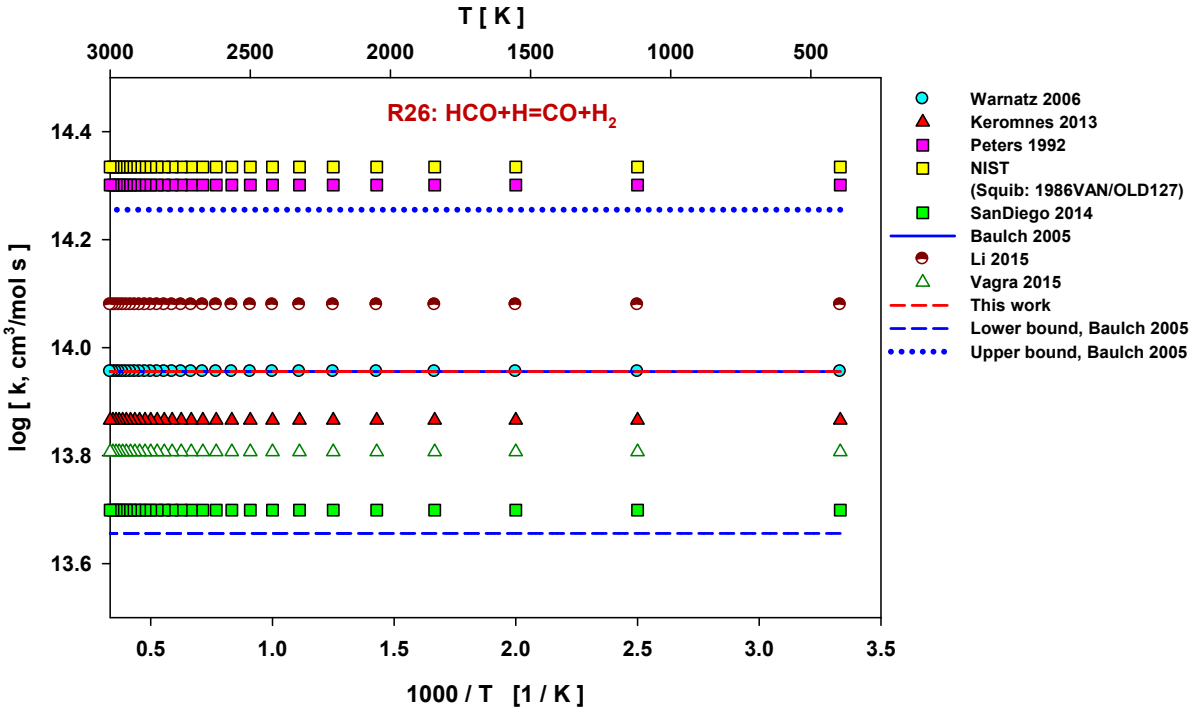

Figure S3.25: Rate constant comparison of reaction R26: $HCO+H = CO+H_2$ from different authors.

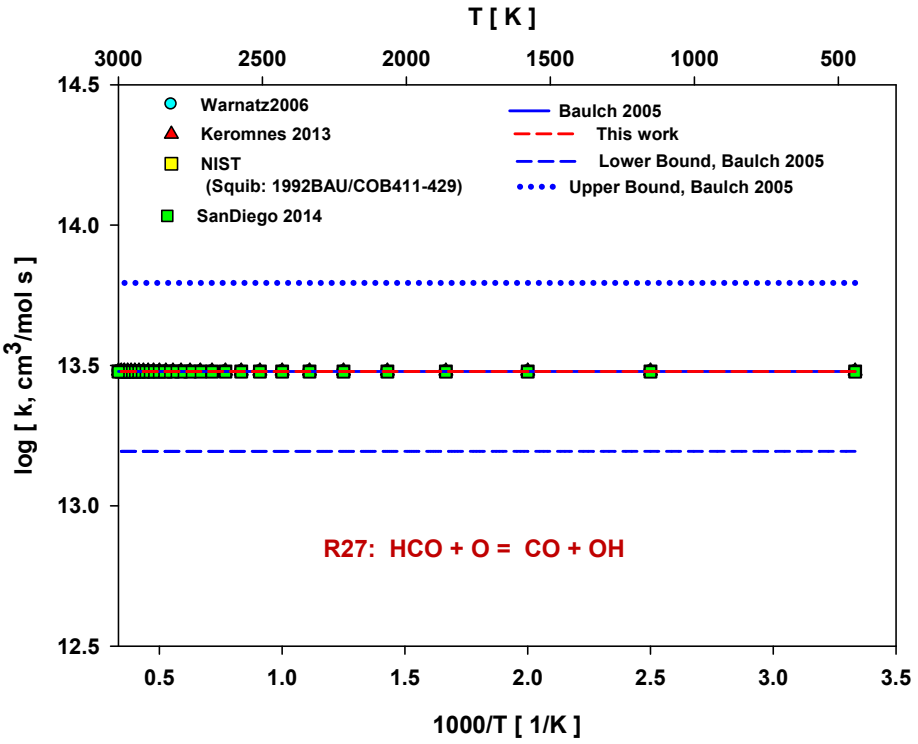

Figure S3.26: Rate constant comparison of reaction R27: HCO+O =CO+OH from different authors.

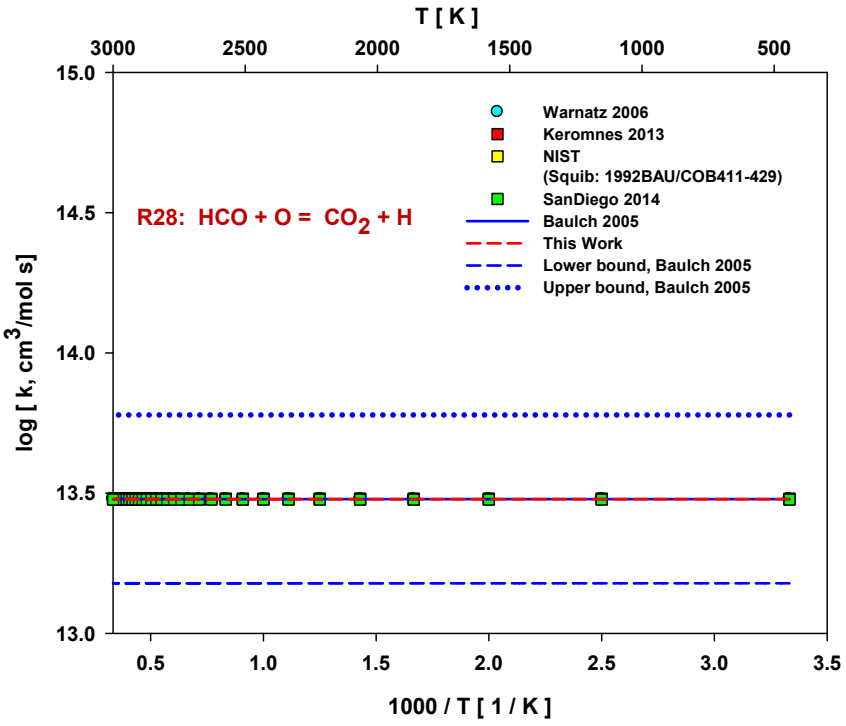

Figure S3.27: Rate constant comparison of reaction R28: HCO+O =CO_2+H from different authors.

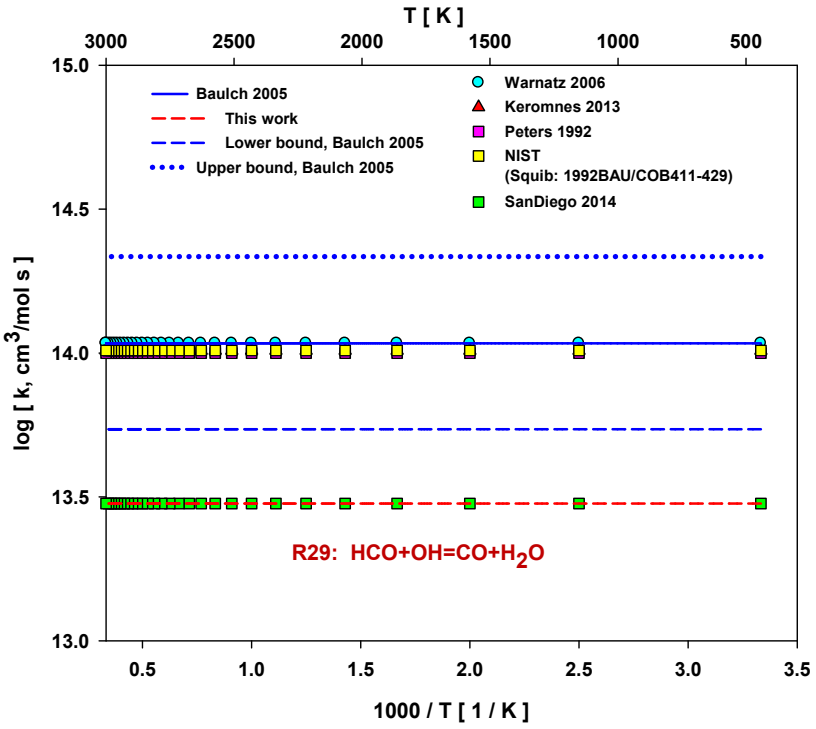

Figure S3.28: Rate constant comparison of reaction R29: HCO+OH =CO+H_2O from different authors.

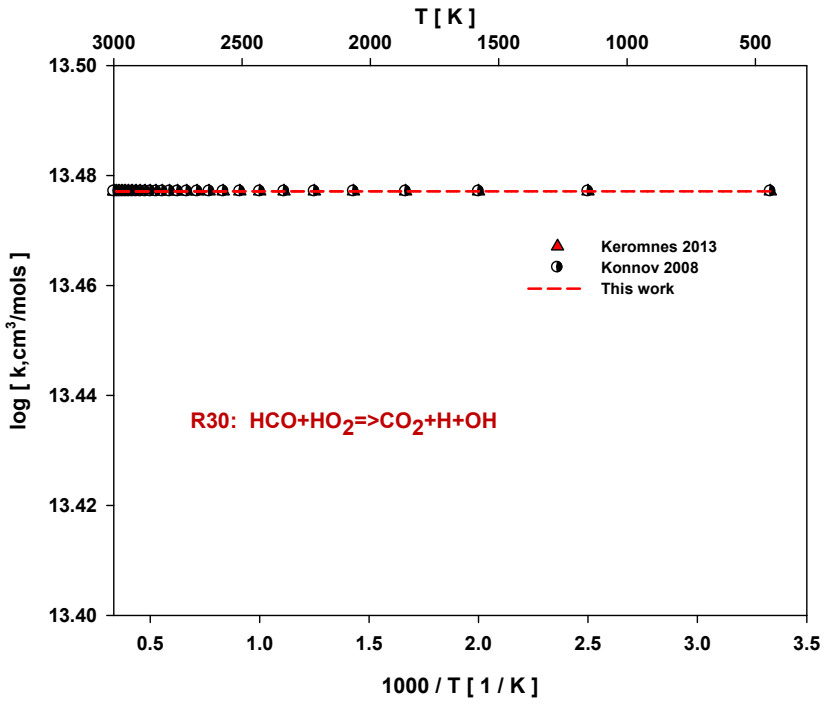

Figure S3.29: Rate constant comparison of reaction R30: HCO+HO_2 =>CO_2+H+OH from different authors.

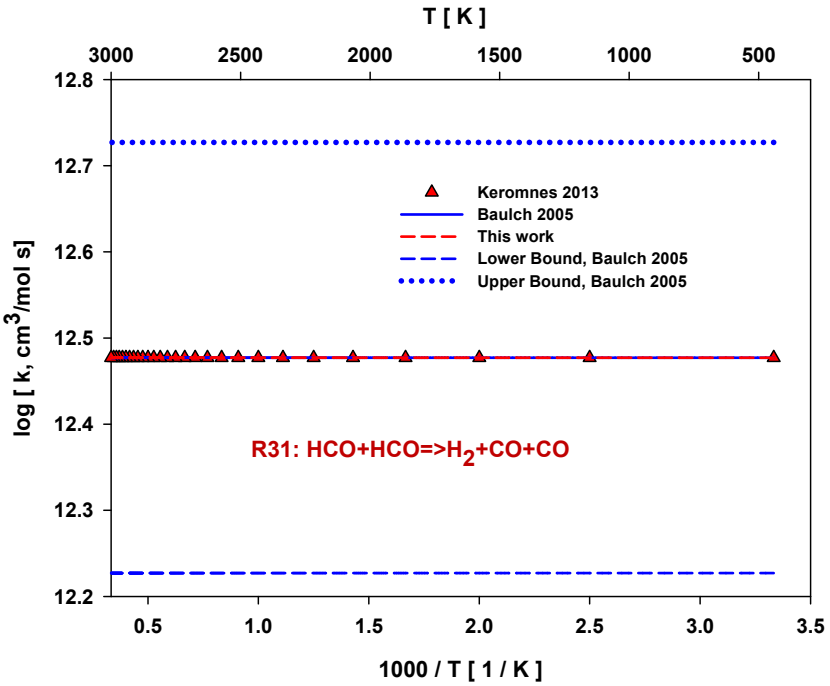

Figure S3.30: Rate constant comparison of reaction R31: HCO+HCO =>H_2+CO+CO from different authors.

References

(1) Http://logesoft.com/loge-software/. http://logesoft.com/loge-software/.

(2) Lee, J. H.; Lee, S. I.; Kwon, O. C. *Int. J. Hydrogen Energy* **2010**, *35* (20), 11332–11341.

(3) Li, J.; Huang, H.; Kobayashi, N.; He, Z.; Nagai, Y. *Int. J. ENERGY Res.* **2014**, *38*, 1214–1223.

(4) Checkel, M. D.; Ting, D. S. K.; Bushe, W. K. *J. Loss Prev. Process Ind.* **1995**, *8* (4), 215–220.

(5) Hayakawa, A.; Goto, T.; Mimoto, R.; Arakawa, Y.; Kudo, T.; Kobayashi, H. *Fuel* **2015**, *159*, 98–106.

(6) Powell, O. A.; Papas, P.; Dreyer, C. *Combust. Sci. Technol.* **2009**, *181* (7), 917–936.

(7) Mathieu, O.; Petersen, E. L. *Combust. Flame* **2015**, *162* (3), 554–570.

(8) Mathieu, O.; Levacque, A.; Petersen, E. L. *Int. J. Hydrogen Energy* **2012**, *37* (20), 15393–15405.

(9) Hidaka, Y.; Takuma, H.; Suga, M. *J. Phys. Chem.* **1985**, *89* (23).

(10) Mathieu, O.; Levacque, A.; Petersen, E. L. *Proc. Combust. Inst.* **2013**, *34* (1), 633–640.

(11) Kopp, M.; Brower, M.; Mathieu, O.; Petersen, E.; Güthe, F. *Appl. Phys. B Lasers Opt.* **2012**, *107* (3), 529–538.

(12) Dayma, G.; Dagaut, P. *Combust. Sci. Technol.* **2006**, *178* (2), 1999–2024.

(13) Dagaut, P.; Lecomte, F.; Mieritz, J.; Glarborg, P. *Int. J. Chem. Kinet.* **2003**, *35* (x), 564–575.

(14) Allen, M. T.; Yetter, R. A.; Dryer, F. L. *Combust. Flame* **1998**, *112*, 302–311.

(15) Glarborg, P.; Kubel, D.; Kristensen, P. G.; Hansen, J.; Dam-Johansen, K. *Combust. Sci. Technol.* **1995**, *110–111* (1), 461–485.

(16) Bian, J.; Vandooren, J.; Van Tiggelen, P. J. *Twenty third Symp. Combust.* **1990**, 379–386.

(17) Vandooren, J.; Bian, J.; Van Tiggelen, P. J. *Combust. Flame* **1994**, *98* (4), 402–410.

(18) Duynslaegher, C.; Jeanmart, H.; Vandooren, J. *Proc. Combust. Inst.* **2009**, *32 I* (1), 1277–1284.

(19) Sausa, R. C.; Singh, G.; Lemire, G. W.; Anderson, W. R. *Twenty-Sixth Symp. Combust.* **1996**, 1043–1052.

(20) Dindi, H.; Tsai, H. M.; Branch, M. C. *Combust. Flame* **1991**, *87* (1), 13–20.

(21) Mathieu, O.; Pemelton, J. M.; Bourque, G.; Petersen, E. L. *Combust. Flame* **2015**, *162* (8), 3053–3070.

(22) Dagaut, P.; Nicolle, A. *Combust. Flame* **2005**, *140* (3), 161–171.

(23) Dagaut, P.; Glarborg, P.; Alzueta, M. U. *Prog. Energy Combust. Sci.* **2008**, *34* (1), 1–46.

(24) Lamoureux, N.; Merhubi, H. El; Pillier, L.; de Persis, S.; Desgroux, P. *Combust. Flame* **2016**, *163*, 557–575.

(25) Baulch, D. L.; Bowman, C. T.; Cobos, C. J.; Cox, R. A.; Just, T.; Kerr, J. A.; Pilling, M. J.; Stocker, D.; Troe, J.; Walker, R. W.; Warnatz, J.; Baulch, D. L. *J. Phys. Chem. Ref. Data 34* **2005**, *757*.

(26) Warnatz, J.; Maas, U.; Dibble, R. W. *Combuation : Physical and Chemical Fundamentals, Modeling and Simulation, Experiments, Pollutant Formation*; Springer Verlag, 2006.

(27) Kéromnès, A.; Metcalfe, W. K.; Heufer, K. A.; Donohoe, N.; Das, A. K.; Sung, C.; Herzler, J.; Naumann, C.; Griebel, P.; Mathieu, O.; Krejci, M. C.; Petersen, E. L.; Pitz, W. J.; Curran, H. J. *Combust. Flame* **2013**, *160*, 995–1011.

(28) Peters, N. *Lecture Notes in Physics : Part I*; Springer Verlag, 1993.

(29) Manion, J. A.; Huie, R. E.; Levin, R. D.; Burgess Jr., D. R.; Orkin, V. L.; Tsang, W.; McGivern, W. S.; Hudgens, J. W.; Knyazev, V. D.; Atkinson, D. B.; Chai, E.; Tereza, A. M.; Lin, C.-Y.; Allison, T. C.; Mallard, W. G.; Westley, F.; Herron, J. T.; Hampson, R. F.;

Frizzell, D. H. NIST Chemical Kinetics Database, NIST Standard Reference Database 17, Version 7.0 (Web Version), Release 1.6.8, Data version 2015.12, National Institute of Standards and Technology, Gaithersburg, Maryland, 20899-8320, 2015.

(30) *"Chemical-Kinetic Mechanisms for Combustion Applications", San Diego Mechanism web page, Mechanical and Aerospace Engineering (Combustion Research),*; 2014.

(31) Starik, A. M.; Titova, N. S.; Sharipov, A. S.; Kozlov, V. E. *Combust. Explos. Shock Waves* **2010**, *46* (5), 491–506.

(32) Konnov, A. A. *Combust. Flame* **2008**, *152*, 507–528.

(33) Varga, T.; Olm, C.; Nagy, T.; Zse´ly, I. G.; Valko, E.; Robert, P. álv´olgyi; Curran, H. J.; Turányi, T. *Int. J. Chem. Kinet.* **2016**, *48*, 407–422.

(34) Hong, Z.; Vasu, S. S.; Davidson, D. F.; Hanson, R. K.; Ref, J. J. P. C. *J. Phys. Chem. A* **2010**, *114*, 5520–5525.

(35) Hong, Z.; Davidson, D. F.; Hanson, R. K. *Combust. Flame* **2011**, *158* (4), 633–644.

(36) Hong, Z.; Lam, K.; Sur, R.; Wang, S.; Davidson, D. F.; Hanson, R. K. *Proc. Combust. Inst.* **2013**, *34* (1), 565–571.

(37) Mueller, M. A.; Yetter, R. A.; Dryer, F. L. *Int. J. Chem. Kinet.* **1999**, *31* (2), 705–724.

(38) Burke, M. P.; Chaos, M.; Ju, Y.; Dryer, F. L.; Klippenstein, S. J. *Int. J. Chem. Kinet.* **2012**, *44*, 444–474.

(39) Burke, M. P.; Klippenstein, S. J.; Harding, L. B. *Proc. Combust. Inst.* **2013**, *34*, 547–555.

(40) Li, X.; You, X.; Wu, F.; Law, C. K. *Proc. Combust. Inst.* **2015**, *35* (1), 617–624.

(41) Sun, H.; Yang, S. I.; Jomaas, G.; Law, C. K. *Proc. Combust. Inst.* **2007**, *31*, 439–446.

(42) Li, J.; Zhao, Z.; Kazakov, A.; Chaos, M.; Dryer, F. L.; Scire, J. J. *Int. J. Chem. Kinet.* **2007**, *39*, 109–136.

(43) Davis, S. G.; Joshi, A. V; Wang, H.; Egolfopoulos, F. *Proc. Combust. Inst.* **2005**, *30*, 1283–1292.

(44) Troe, J. *Combust. Flame* **2011**, *158* (4), 594–601.